The Sensitivity of the Fitch Wind Farm Parameterization to a Three-Dimensional Planetary Boundary Layer Scheme

Alex Rybchuk[1,2], Timothy W. Juliano[3], Julie K. Lundquist[1,4], David Rosencrans[1,4], Nicola Bodini[1], and Mike Optis[1]

[1]National Renewable Energy Laboratory, Golden, Colorado, USA
[2]Department of Mechanical Engineering, University of Colorado Boulder, Boulder, Colorado, USA
[3]Research Applications Laboratory, National Center for Atmospheric Research, Boulder, Colorado, USA
[4]Department of Atmospheric and Oceanic Sciences, University of Colorado Boulder, Boulder, Colorado, USA

Correspondence: A. Rybchuk (alex.rybchuk@nrel.gov)

Abstract. Wind plant wake impacts can be estimated with a number of simulation methodologies, each with its own fidelity and sensitivity to model inputs. In turbine-free mesoscale simulations, hub-height wind speeds often significantly vary with the choice of a planetary boundary layer (PBL) scheme. However, the sensitivity of wind plant wakes to a PBL scheme has not been explored because, as of the Weather Research and Forecasting model v4.3.3, wake parameterizations were only compatible with one PBL scheme. We couple the Fitch wind farm parameterization with the new NCAR 3DPBL scheme and compare the resulting wakes to those simulated with a widely used PBL scheme. ~~First, we~~ We simulate a wind plant in pseudo-steady states under idealized stable, neutral, and unstable conditions with matching hub-height wind speeds using two PBL schemes: MYNN and the NCAR 3DPBL. For these idealized scenarios, average hub-height wind speed losses within the plant differ between PBL schemes by ~~±0.24~~ between -0.20 m s^{-1} and 0.22 m s^{-1}, and correspondingly, capacity factors ~~ranged~~ range between 39.5~~–51.2%. To demonstrate the importance of PBL scheme choice on a real-world scenario, we conduct a month-long case study with both PBL schemes centered on the Vineyard Wind 1 lease area in the mid-Atlantic United States. Under stable and unstable conditions averaged across the month, MYNN predicts stronger waking inside the plant—by about 0.25 m s⁻¹. However, due to stronger plant inflow wind speeds in MYNN, the 3DPBL generates 4.7%–7~~–53.8%~~less power than MYNN in August 2020, depending on the turbine build-out scenario. Differences between PBL schemes can be even larger for individual instances in time.~~. These simulations suggest that PBL schemes represent a meaningful source of modeled wind resource uncertainty; therefore, we recommend incorporating PBL variability into future wind plant planning sensitivity studies as well as wind forecasting studies.

Copyright statement. This work was authored in part by the National Renewable Energy Laboratory, operated by Alliance for Sustainable Energy, LLC, for the U.S. Department of Energy (DOE) under Contract No. DE-AC36-08GO28308. Funding provided by the U.S. Department of Energy Office of Energy Efficiency and Renewable Energy Wind Energy Technologies Office and by the National Offshore Wind Research and Development Consortium under Agreement No. CRD-19-16351. The views expressed in the article do not necessarily represent the views of the DOE or the U.S. Government. The U.S. Government retains and the publisher, by accepting the article for publication, acknowledges that the U.S. Government retains a nonexclusive, paid-up, irrevocable, worldwide license to publish or reproduce the published form of this work, or allow others to do so, for U.S. Government purposes.

1 Introduction

Despite a large demand to build offshore wind turbines in the United States, the wind resource at many potential construction sites suffers from a large degree of uncertainty. Wind resource assessments for new wind plants often involve gathering multi-year measurements of hub-height winds (Brower et al., 2012). While this approach is ~~more~~ common for onshore sites, hub-height wind measurements are more challenging to collect offshore, and public offshore measurements are sparse within the United States. While the Bureau of Offshore Energy Management (BOEM) is considering or has already allowed commercial development in 33 renewable energy areas (BOEM, 2020), to the best of the authors' knowledge, public offshore yearlong hub-height wind speed measurements are available today in the vicinity of 6 sites—4 due to deployments by the U.S. DOE (accessible at https://a2e.energy.gov/data) and 2 due to deployments by the New York State Energy Research and Development Agency (accessible at https://oswbuoysny.resourcepanorama.dnvgl.com). The U.S. is rapidly developing its offshore wind industry, recently expanding its offshore wind generation goal to 30 GW by 2030 (White House, 2021). Thus, it is critical to be able to accurately and confidently characterize wind resource in the absence of high quality measurements for the rapidly developing offshore wind industry in the United States.

Due to limited observations, offshore wind resource assessments in the United States rely more heavily on numerical weather prediction (NWP) models. NWP-based wind resource assessments have been used to characterize wind resource in turbine-free environments (simulating winds prior to wind plant construction) as well as turbine-including environments (simulating winds after wind plant construction). While NWP models provide useful predictions of wind resource, their estimates are also accompanied by a large degree of uncertainty. As such, uncertainty quantification of offshore wind resource has been established as a key component of the U.S. offshore wind research agenda. Shaw et al. (2019) assert that uncertainty quantification represents a critical area of offshore wind research, as "quantification and reduction of uncertainty represents a significant opportunity to reduce costs". This sentiment was also echoed in a wind energy workshop that brought together stakeholders from industry, academia, and the U.S. government (Haupt et al., 2020). Finally, Archer et al. (2014) underscored two major research needs for coastal and offshore wind energy research in the United States—more offshore observations and uncertainty characterization, in particular uncertainty characterization through ensembles of NWP simulations. Archer et al. (2014) also emphasized the need for research on turbine wake losses. The research in our manuscript directly responds to the need for ensembles of NWP simulations as well the need to quantify wake losses.

Wind resource uncertainty in turbine-free NWP simulations stems from, in part, the large number of plausible model options that can be used to drive the simulation. Hub-height wind speeds in turbine-free NWP simulations have been shown to be significantly sensitive to a number of modeling options. Simulated wind resource has been shown to often be most sensitive to the choice of ~~plantary~~ planetary boundary layer (PBL) parameterization, and PBL schemes have also been shown to be sensitive to other factors such as grid resolution (Storm and Basu, 2010; Carvalho et al., 2012; Yang et al., 2013; Carvalho et al., 2014;

Draxl et al., 2014; Olsen et al., 2017; Yang et al., 2017; Fernández-González et al., 2018; Yang et al., 2019; Optis et al., 2020). PBL schemes govern turbulent fluxes (typically just vertical turbulent fluxes) and mixing within the atmospheric boundary layer. At present, 13 different PBL schemes are available within the Weather Research and Forecasting (WRF, Skamarock et al., 2021) model, and there is no single-best PBL scheme for wind resource assessment. As just one example, Draxl et al. (2014) evaluated seven PBL schemes using measurements from a meteorological mast at the Høvsøre wind energy test site. They found that the optimal PBL scheme varies with stability: at this site, MYJ (Janjić, 1994) performed best under stable conditions, ACM2 (Pleim, 2007) performed best under neutral conditions, and YSU (Hong et al., 2006) performed best under unstable conditions. Wind atlases that characterize model uncertainty often employ ensembles of simulations where model inputs, such as PBL scheme, are varied (Bodini et al., 2021a).

While the sensitivity of hub-height winds to PBL scheme has been explored in turbine-free NWP simulations, the resulting impacts on wake simulations have not been explored. To date, all published mesoscale WRF simulations with explicitly represented wind turbines have been conducted with the MYNN PBL scheme (Nakanishi and Niino, 2009; Olsen et al., 2017). Thus, while PBL schemes have been shown to be key elements for uncertainty quantification in NWP-based wind resource assessments in turbine-free environments, it is unknown if PBL schemes are similarly important in turbine-including environments. It is critical to accurately predict wake effects in order to accurately predict annual energy production. Lee and Fields (2021) summarize the large degree of uncertainty regarding the impact of wake-associated losses on annual energy production: Some estimates predict average total wake losses as low as 6.1%, whereas others have predicted losses as high as 40%. The uncertainty of individual wake-loss estimates has also been estimated to be 10%–40%. These losses and uncertainties incur significant financial impact on the wind industry, potentially translating to millions of U.S. dollars of economic benefits (Lee and Fields, 2021).

While turbine-including NWP sensitivity studies have not examined the impact of PBL schemes on mesoscale wakes, they have shown that NWP-modeled wakes can be sensitive to a number of other inputs. Turbine wakes are modeled in NWP simulations with wind farm parameterizations (WFPs, for a review see Fischereit et al., 2021), such as the Fitch WFP (Fitch et al., 2012), the Explicit Wake Parametrisation (EWP, Volker et al., 2015), ~~the Abkar WFP (Abkar and Porté-Agel, 2015), and the Pan~~ and the hybrid WFP (Pan and Archer, 2018). Wind resource in turbine-including simulations has been shown to be sensitive to the same model inputs that are important in turbine-free simulations, such as vertical and horizontal grid resolution, as well as the option to have the MYNN PBL scheme advect TKE (Redfern et al., 2019; Tomaszewski and Lundquist, 2020; Archer et al., 2020; Siedersleben et al., 2020; Larsén and Fischereit, 2021). We note that ~~some~~ most if not all Fitch WFP simulations with TKE advection turned on prior to Archer et al. (2020) were subject to a bug in the WRF code, and as such, the results from these studies should be interpreted with caution. Modeled wake impacts have also been shown to be sensitive to inputs specifically associated with the WFP, such as the choice of WFP and the degree of explicitly added TKE in the Fitch WFP (Fitch et al., 2012; Vanderwende et al., 2016; Siedersleben et al., 2020; Tomaszewski and Lundquist, 2020; Archer et al., 2020; Pryor et al., 2020; Shepherd et al., 2020).

In this paper, we begin to address the question: How sensitive are modeled mesoscale wakes to the choice of PBL parameterization? ~~Specifically, we compare Fitch WFP simulations with both~~ Ideally, this question would be addressed by studying all 13 PBL schemes in WRF with the Fitch WFP insofar as that is possible. Here, as a first step, we compare two PBL schemes: MYNN (Nakanishi and Niino, 2009) and the recently developed NCAR 3DPBL ~~(Kosović et al., 2020; Juliano et al., 2021). We~~ (Kosović et al., 2020; Juliano et al., 2022). We chose the latter as it has a prognostic equation for TKE, which is important as the Fitch WFP modifies TKE fields. We make substantial modifications to the WRF code to enable the Fitch WFP to work with the NCAR 3DPBL, and then conduct ~~two sets of numerical experiments. We are most interested in the sensitivity of modeled wakes in upcoming offshore U.S. wind plants introduced by switching from MYNN to the 3DPBL. As such, we simulate a month-long case study centered on planned wind plants off the U. S. east coast. Prior to discussing this dynamic and complicated environment, we first~~ a set of idealized numerical experiments based on the Fitch et al. (2012) experiments. We simulate wakes in pseudo-steady idealized environments with MYNN and the NCAR 3DPBL under stable, neutral, and unstable conditions. We also examine the role of explicitly added TKE in this set of simulations. In Section 2, we describe the two PBL schemes, the integration of the NCAR 3DPBL with the Fitch WFP in the WRF code, and the setup of the simulations. In Section 3, we discuss the results of the ~~idealized~~ simulations. In Section 4, we ~~analyze the real simulations. In Section 5, we conclude and present broader takeaways~~conclude and discuss the implications of the idealized results for real-world wind resource assessments.

2 Methods

2.1 MYNN and the NCAR 3DPBL

The simulations in this paper are carried out using WRF v4.3.0 with two PBL schemes: MYNN (Nakanishi and Niino, 2009; Olson et al., 2019) and the NCAR 3DPBL ~~(Kosović et al., 2020; Juliano et al., 2021)~~(Kosović et al., 2020; Juliano et al., 2022) . To avoid confusion regarding nomenclature of new turbulence models, we note that the NCAR 3DPBL is different from the 3DTKE PBL scheme (Zhang et al., 2018). The WRF v4.3.0 code in this study was modified to include the NCAR 3DPBL code, which is being prepared for public release. For simplicity, we refer to the NCAR 3DPBL as simply "the 3DPBL." Both MYNN and the 3DPBL share a common origin—they are fundamentally rooted in the turbulence modeling of Mellor and Yamada (1974). Here, we use the level 2.5 MYNN and 3DPBL schemes, which both treat TKE as a prognostic variable, thus improving their utility for wind turbine modeling, because generated TKE is advected by the PBL schemes. This behavior stands in contrast to other PBL schemes, such as YSU, which does not treat TKE as a prognostic variable.

MYNN and the 3DPBL treat turbulent mixing differently. MYNN computes the vertical turbulent mixing by calculating the vertical turbulent stress divergence, and it allows the horizontal turbulent mixing to be handled externally with a Smagorinsky-type approach (Skamarock et al., 2021, Sec. 4.2). In contrast, the 3DPBL directly accounts for horizontal turbulent mixing by explicitly computing the turbulent flux divergences for momentum, heat, and moisture. The 3DPBL has been implemented into WRF to allow for three different configurations following the original Mellor-Yamada developments: (*i*) a full 3D model, (*ii*) a quasi-3D model using the so-called PBL-approximation, and (*iii*) a 1D model using the PBL-approximation. In this analysis, we employ the second option, as the full 3D parameterization is currently too computationally expensive for ~~the month-long mid-Atlantic simulations~~yearlong wind resource assessments. When using the second option, the 3DPBL scheme handles both the vertical and horizontal turbulent mixing by computing the 3D turbulent stress divergence, in addition to the 3D turbulent flux divergence of heat and moisture. The vertical turbulent fluxes in the 3DPBL are calculated similarly to MYNN, and the horizontal turbulent fluxes are calculated analytically following Mellor and Yamada (1982) after applying the PBL approximation (i.e., neglecting the horizontal derivatives of mean quantities in addition to the vertical derivative of vertical velocity).

Aside from different approaches for horizontal mixing, the two PBL schemes also employ different master length scales and closure constants. Both schemes employ one "master" length scale, although they calculate them differently. In the simulations in this study, the 3DPBL master length scale follows Mellor and Yamada (1982), whereas the MYNN master length scale uses a different approach that simultaneously accounts for length scales that characterize buoyancy, the surface layer, and the PBL depth. The closure constants for the 3DPBL length scale come from Mellor and Yamada (1982), whereas the MYNN closure constants were updated in Nakanishi and Niino (2009). ~~The MYNN updates focused on convective conditions and, as such, we expect (and find) that the two PBL schemes behave most differently in convective conditions.~~

While the values of empirical constants are different, MYNN and the quasi-3DPBL use the same formulation to parameterize turbulent momentum, heat, and moisture fluxes. For example, they parameterize the vertical flux of the u-component of wind speed as

$$\langle uw \rangle = -LqS_m \frac{\partial U}{\partial z}, \tag{1}$$

where L is the master length scale, q is $\sqrt{2\,\mathrm{TKE}}$, S_m is a stability function, and U is zonal velocity (Mellor and Yamada, 1982).

2.2 Integration of the Fitch WFP with the 3DPBL

To simulate wakes with the 3DPBL, we first integrated the Fitch WFP with the 3DPBL inside the WRF code. The Fitch WFP modifies flow in two key manners (Fitch et al., 2012; Archer et al., 2020): by slowing winds

$$\frac{\partial u_k}{\partial t} = -\frac{1}{2}\frac{A_k C_T U_k u_k}{z_{k+1} - z_k} \tag{2}$$

$$\frac{\partial v_k}{\partial t} = -\frac{1}{2}\frac{A_k C_T U_k v_k}{z_{k+1} - z_k} \tag{3}$$

and by adding TKE

$$\frac{\partial \mathrm{TKE}_k}{\partial t} = \frac{1}{2}\frac{A_k \alpha C_{TKE} U_k^3}{z_{k+1} - z_k}. \tag{4}$$

In the above equations, k is the vertical level that intersects the rotor, A_k is the area of the rotor on this vertical level, C_T is the thrust coefficient, U_k is the wind speed, u_k is the zonal wind, v_k is the meridional wind, and z_k is the height. The turbulence

Stability	~~Label~~ PBL Scheme	Geostrophic Wind Speed [m s^{-1}]	Surface Heat Flux [W m~~−2~~$^{-2}$]	Spin Up Duration [days]	Final ABL Heig
Stable	~~NWF~~ MYNN	10	-15	6	250
Stable	~~NWF~~ 3DPBL	10	-15	~~4.25~~ 5.25	250
Neutral	~~NWF~~ MYNN	10	0	4	550
Neutral	~~NWF~~ MYNN	10	0	4	550
Unstable	~~NWF~~ MYNN	9	20	2	600
Unstable	~~NWF~~ 3DPBL	10	20	2	600

Table 1. A summary of boundary conditions and spinup times for the turbine-free idealized simulations.

coefficient C_{TKE} is calculated as the difference between the thrust coefficient C_T and the power coefficient C_P. The thrust and power coefficients are functions of wind speed that are unique to a particular wind turbine, and their values are specified in the input file *wind-turbine.tbl*. The coefficient α was introduced by Archer et al. (2020) to empirically modify the amount of explicit TKE addition and, in this study, we either set it to 0 or 1.

The major challenge in integrating the Fitch WFP and the 3DPBL is that the 3DPBL code is housed in the dynamics (*dyn_em/*) part of the code, as opposed to the physics (*phys/*) part of the code where most other PBL schemes reside. As such, the codebase was substantially modified to account for the user-selected PBL scheme. A call to the Fitch WFP's *dragforce* subroutine was added to the end of *dyn_em/module_first_rk_step_part2.F*. When called for the 3DPBL, the velocity tendencies and TKE tendencies are additionally scaled by the column-mass in order to match the identical scaling that happens to the *phys/*-calculated tendencies earlier within *dyn_em/module_first_rk_step_part2.F*. Additionally, whereas the Fitch WFP code modifies the MYNN TKE field directly (including a timestep factor of ∂t), the new code modifies the 3DPBL TKE tendency field (omitting a factor of ∂t and letting the rest of the code carry out the time integration).

2.3 Configuration of ~~Idealized~~ Simulations

~~First, we~~ We carry out a series of idealized simulations to study the effect of the PBL scheme on simulated wake dynamics in a simple offshore environment. All simulation inputs can be found on Zenodo (https://doi.org/10.5281/zenodo.5565399). We use the neutral idealized simulations of Fitch et al. (2012) as inspiration for our simulations, but we make a number of modifications. All simulations use two domains, each 202-by-202 grid points in the horizontal. MYNN is always used in the outer domain, whereas the inner domain is either MYNN or the 3DPBL. The outer domain uses a horizontal grid spacing of 3 km and a timestep of 9 seconds, whereas the inner domain uses a horizontal grid spacing of 1 km and a timestep of 3 seconds. The vertical grid uses 81 cells, up to a height of 20 km. Vertical grid stretching is employed to provide finer resolution near the surface, thereby allowing 28 vertical levels below a height of 300 m, following the recommendation of Tomaszewski and Lundquist (2020) for nominally 10 m of resolution near the surface. All simulations have a roughness length of 0.0001 m, which is characteristic of offshore environments (Stull, 1988).

In order to eventually simplify wake comparisons, we force all turbine-free simulations in such a manner that average hub-height wind speeds are roughly equal ($\sim$9.35 m s^{-1}) after they are spun up (Table 1). In principle, we could have matched the geostrophic winds instead of the hub-height winds in the idealized simulations, but the resulting different hub-height wind speeds would have made it more difficult to isolate the different turbulent recovery effect that comes with using the 3DPBL instead of MYNN. ~~Under ideal circumstances, the MYNN and 3DPBL simulations would all have the same geostrophic winds and hub-height wind speeds. But this behavior is not always possible to achieve because different PBL schemes will inherently produce different wind profiles. As such, in the idealized simulations we match hub-height wind speeds, but we explore the effects of matching large-scale forcing in the mid-Atlantic analysis. For a greater discussion of the spinup of the idealized simulations, see Sec. 3.1.~~

Simulations for each stability case are initialized with a neutral temperature profile of 285 K within the boundary layer up to 500 m. The boundary layer is capped with a two-layer inversion: a strong inversion (5 K warming between 500 m and 600 m) and a weaker inversion (3 K km^{-1} lapse rate above 600 m). Depending on the case, each simulation was forced with either 9 m s^{-1} or 10 m s^{-1} geostrophic winds. Stable simulations are additionally forced with -15 W m^{-2} surface cooling, and unstable simulations are forced with 20 W m^{-2} surface heating. These sensible heat flux values were chosen based on typical simulated conditions at ~~Vineyard Wind (Sec.??)~~a planned offshore plant in the U.S. mid-Atlantic (Rybchuk, 2022), and are smaller than typical values over land. After spin up, the boundary-layer height as determined through the NWF temperature profile (Fig. 2) is approximately 250 m in the stable simulations, 550 m in the neutral simulations, and 600 m in the unstable simulations.

After spinning up turbine-free simulations, we run three cases of simulations for each of the stabilities and each of the PBL schemes for 24 hours. The first case is simply a continuation of the turbine-free simulations and is referred to as the no-wind-farm (NWF) case. The second case (100TKE) starts after the respective NWF simulation has spun up and shares its boundary conditions, but it includes a 10-by-10 grid of turbines based on the 12-MW International Energy Agency (IEA, Beiter et al., 2020) reference offshore wind turbines placed in the center of the inner domain. The turbine hub-height is 138 m, and the rotor diameter is 215 m. Cut-in speed is 3 m s^{-1}, rated speed is 10.9 m s^{-1}, and cut-out speed is 30 m s^{-1}. Turbines are placed 2 km apart, which is close to the 1 nautical mile spacing used in the real simulations. In this case, 100% of explicit TKE is generated by the Fitch WFP ($\alpha = 1$). In the third case (0TKE), we explore the sensitivity to explicitly added TKE by duplicating the setup of the second case, but turning off explicit TKE generation ($\alpha = 0$).

2.4 ~~Configuration of Real Simulations~~

~~(a) The inner and outer domain of the mid-Atlantic simulations. Lease areas are shown along the coastline of the inner domain. An expanded view of the lease areas is available at BOEM (2020). (b) The turbine layout in the vicinity of Vineyard Wind 1. This plant is enclosed by a gray boundary.~~

~~Label Short Description NWF No-wind-farm simulation LEASE A simulation that contains turbines in all discussed Lease Areas VW-ONLY A simulation that contains turbines only at Vineyard Wind 1 A summary of different real simulation cases. Each of these cases was run with both MYNN and the 3DPBL.~~

~~Next, to address the question "Is it worthwhile for future offshore wake sensitivity studies to vary PBL scheme?", we study wake sensitivity centered on planned offshore wind plants off the U.S. east coast (Fig. **??**). The domain is centered on the mid-Atlantic, focused on waters off the coast of Maryland, Delaware, New Jersey, New York, Connecticut, Rhode Island, and Massachusetts. We run three cases of real simulations for both of the PBL schemes (Table **??**). The first case simulates a turbine-free atmosphere and is referred to as the NWF case. The second case simulates turbines in all of the lease areas within the domain as defined by the Bureau of Offshore Energy Management (BOEM) on March 3, 2020 (BOEM, 2020) . As such, 14 lease areas are included, ranging from US Wind Inc. in the south to the cluster of lease areas near Rhode Island and Massachusetts in the north. This case is called LEASE. The third case is the same as the second case, but it only simulates the Vineyard Wind 1 wind plant; it is referred to as VW-ONLY. This third case enables us to differentiate between two types of wakes, as proposed by the International Electrotechnical Commission (IEC) 61400-15 working group (Fields and Sherwin, 2017):~~

1. ~~Internal wakes: These are wake effects that come from within a plant. The wakes at Vineyard Wind 1 in VW-ONLY only come from one farm. As such, we can isolate self-waking in VW-ONLY.~~

2. ~~External wakes: These are wake effects that arrive from outside of a particular plant of interest. The wakes at Vineyard Wind 1 in LEASE come from the Vineyard Wind farm itself as well as the neighboring farms. We can subtract out the internal waking from the VW-ONLY effects to quantify the impact of the neighbors.~~

~~We focus on Vineyard Wind because, at the time the simulations for this study were initiated, it was likely to be first 100+ MW project in US offshore water.~~

~~We simulate winds for the month of August 2020. We chose this period because of its high electricity demand (Livingston and Lundquist, . We start the simulations on July 30, 2020, to allow for 48 hours of spin-up, and we omit this data from analysis. The domain used in this study is identical to the one used by the 20-year NREL mid-Atlantic analysis available at NREL (2020). The outer domain at 6-km grid spacing has 196 grid points in the west-east direction and 122 grid points in the south-north direction and uses a timestep of 18 seconds. The inner domain of 2-km grid spacing has 466 grid points in the west-east direction and 259 in the south-north direction and uses a timestep of 6 seconds. We save data from the inner domain every 5 minutes. As with the idealized simulations, the outer domain for all simulations uses the MYNN PBL scheme, whereas the inner domain either uses MYNN or the 3DPBL. TKE advection is turned on for all MYNN domains. All domains use Thompson microphysics (Thompson et al., 2008), RRTMG for radiation (Iacono et al., 2008), Jiménez-modified Monin-Obukhov for the surface layer scheme (Jiménez et al., 2012), and the unified Noah land-surface model (Tewari et al., 2004). Horizontal turbulent mixing is carried out with a Smagorinsky-diffusion style approach in MYNN, whereas it is calculated from the horizontal turbulent flux divergence in the 3DPBL. ERA5 (Hersbach et al., 2020) provides atmospheric forcing, and OSTIA at 1/10° resolution provides sea surface temperatures (Donlon et al., 2012).~~

~~We select turbines and turbine spacing that are consistent with current expected standards of offshore U.S. wind plants. The mid-Atlantic simulations use the same 12-MW turbine that was used in the idealized simulations. This turbine is similar to the 62 13-MW turbines that are slated for operation in Vineyard Wind 1 (Vineyard Wind, 2021). All modeled lease areas are~~

~~fully built out in order to study the maximum possible power production and wake strength. They are spaced 1 nautical mile apart, which is the same spacing that will be used in Vineyard Wind 1. In total, 177 turbines are modeled in the VW-ONLY simulations, and 1,418 turbines are modeled in the LEASE simulations. We note that the official layout of the Vineyard Wind 1 site was announced after our simulations were completed. The official layout will only include turbines in the northern half of Vineyard Wind 1. As such, our study will overestimate the magnitude of internal waking at Vineyard Wind 1 in the years immediately after it is built. All wind plant simulations are run with $\alpha = 1$. While validation of this parameter is limited, we note that Larsén and Fischereit (2021) saw more accurate results in an offshore wake study with that value than the value of $\alpha = 0.25$ recommended by Archer et al. (2020).~~

3 Results~~: Idealized Simulations~~

3.1 Turbine-Free Conditions

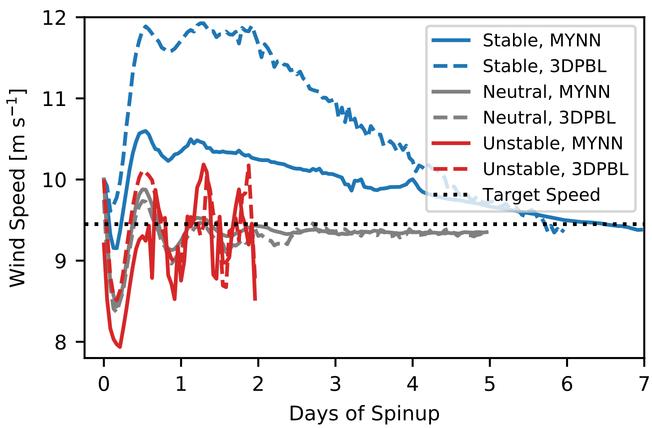

Figure 1. Hub-height wind speed at the center of each domain during spinup in the idealized turbine-free simulations. The last 24 hours of each simulation is taken as the performance period for the NWF simulations.

We spin up the idealized turbine-free simulations so that hub-height wind speeds achieve a psedo-steady state as well as a value of approximately 9.35 m s^{-1} (Fig. 1). As was observed in Fitch et al. (2012), inertial oscillations occur in neutral conditions, but they sufficiently dampen out in our simulations after 4 days. Unstable simulations initially show hub-height wind speed behavior that is similar to the neutral simulations. However, surface warming initiates thermal turbulence during the first day of spinup, and after 24 hours of spinup, the ~~turbulent~~ hub-height wind speed behavior becomes stationary. Stable simulations show an initial hub-height wind speed spike due to the development of a low-level jet (LLJ, Fig. 2), but the wind speeds linearly decay over time as the nose of the LLJ moves upward. The stable MYNN and 3DPBL simulations achieve the target wind speed after 6 and ~~4.25~~ 5.25 days respectively.

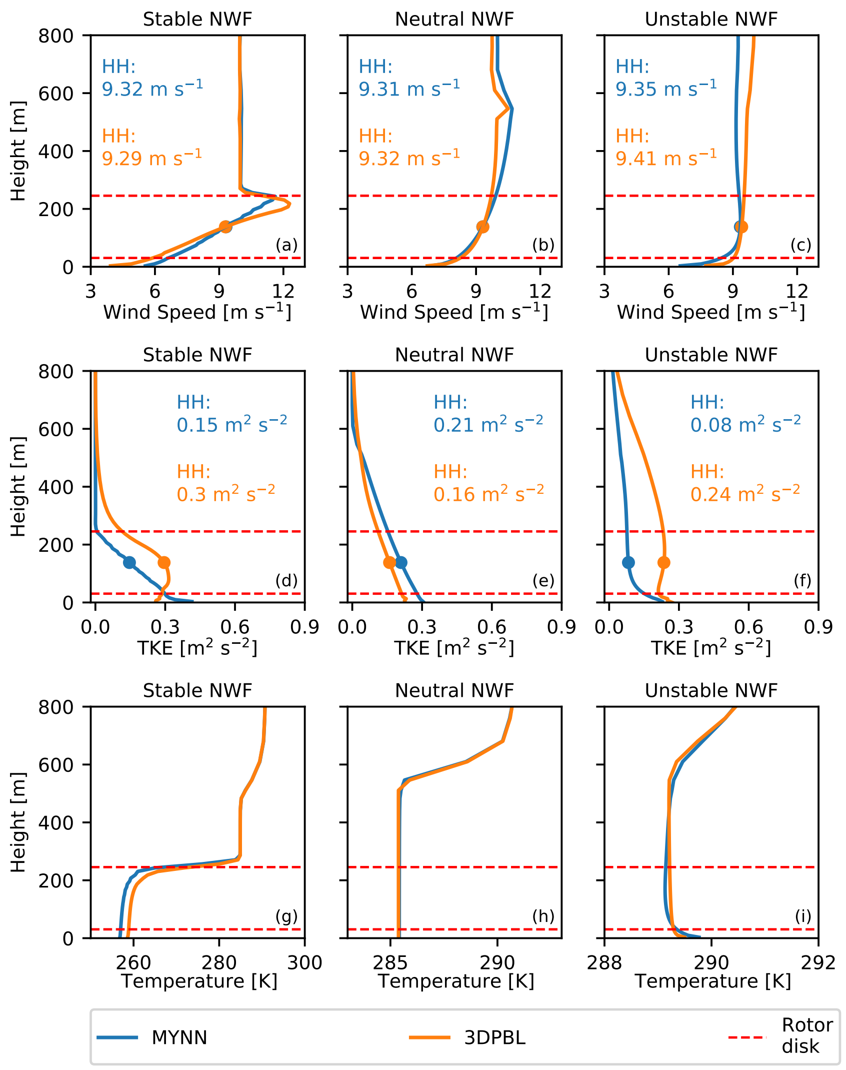

Figure 2. Averaged wind speed profiles (a–c), TKE profiles (d–f), and temperature profiles (g–i) in different stabilities for the idealized NWF runs. Profiles have been horizontally averaged over the extent of the plant and time averaged over the 24 hour performance period. Hub-height values of wind speed and TKE for each PBL scheme are noted.~~The sharp peaks in TKE at the lowest level of the 3DPBL simulations are tied to the staggered representation of TKE in the new PBL scheme, and future versions of the 3DPBL will correct this issue.~~

Having discussed the initial transient phase of the idealized simulations, it is also necessary to characterize the baseline wind speeds and TKE values in the turbine-free simulations (NWF) before analyzing turbine impacts (Fig. 2). The differences and similarities in the wind and TKE profiles of the NWF simulations will dictate the comparison of the wake effects between the PBL schemes in turbine-including simulations. In general, MYNN and the 3DPBL will predict differing wake effects because of two primary factors: different predictions of turbine-free wind speed profiles as well as differing wake recovery behavior, which is linked to parameterizations of turbulent fluxes (Gupta and Baidya Roy, 2021). Due to the experimental configuration of our idealized simulations, the plant inflow wind speeds are similar, and thus we expect the largest wake differences to arise from differing turbulent recovery behavior.

During the performance phase, all simulations have similar average hub-height wind speeds: between 9.3 m s^{-1} and 9.4 m s^{-1}. The wind speed profiles for both PBL schemes match expected canonical behavior for each stability (Stull, 1988). Across the rotor disk, the neutral and unstable wind speed profiles have similar values for both MYNN and the 3DPBL. However in the stable simulations, wind speed profiles slightly differ between the two PBL schemes. The nose of the MYNN low-level jet achieves a wind speed of 11.6 m s^{-1} and sits at the top of the rotor disk. In contrast, the nose of the 3DPBL LLJ achieves a wind speed of ~~12.2~~ 12.3 m s^{-1} and sits about 40 m below the top of the rotor disk. Thus, we will later see that the height of maximum wind speed deficits will differ between the two simulations (Fig. 4).

While MYNN and the 3DPBL produce near-identical TKE profiles in neutral conditions, their TKE profiles differ in stable and unstable conditions. In stable conditions, the MYNN TKE profile linearly decays when moving from the surface to the capping inversion, whereas the 3DPBL profile shows an irregular shape that somewhat resembles the wind speed profile of an LLJ. In unstable conditions, the TKE profiles are relatively constant over the height of the rotor disk, but the 3DPBL TKE values are 2–3 times larger than the MYNN values. Contrary to what might be expected, we note that hub-height values of TKE are weaker in the unstable MYNN simulations than in the neutral MYNN simulations.

3.2 Hub-Height Wind Speed Deficits

~~Internal wakes~~ Wakes within the extent of the plant are sensitive to the choice of PBL scheme, presence of explicit TKE generation, and stability (Fig. 3). We quantify ~~internal wake strength~~ wind speed deficits inside the plant by finding the daylong time-averaged hub-height wind speeds within the plant in the turbine-including simulations ("WFP," which is a generic stand-in for "100TKE" or "0TKE") relative to hub-height winds in the turbine-free simulations ("NWF"). We also calculate the percentage of wind speed loss with reference to the NWF winds inside the plant. Before discussing the impact of PBL scheme, we reiterate that previous work at offshore wind farms demonstrates that stability impacts ~~internal wakes~~ waking (Hansen et al., 2012), and our idealized wakes follow expected trends: stable wakes are strongest (~~1.19~~1.17–1~~.58~~ .54 m s^{-1}, ~~12.5~~12.4–16~~.6~~.3%), followed by neutral wakes (~~0.94~~0.93–1.27 m s^{-1}, 10.0–13.5%), followed by unstable wakes (~~0.87~~0.89–1.19 m s^{-1}, 9.4–12.7%).

Average ~~internal wakes~~ wind speed deficits inside the plant can vary quite substantially between MYNN and the 3DPBL. Across all simulations, MYNN predicts internal ~~wakes that differ~~ waking that differs from the 3DPBL by between ~~-0.24~~ -0.20

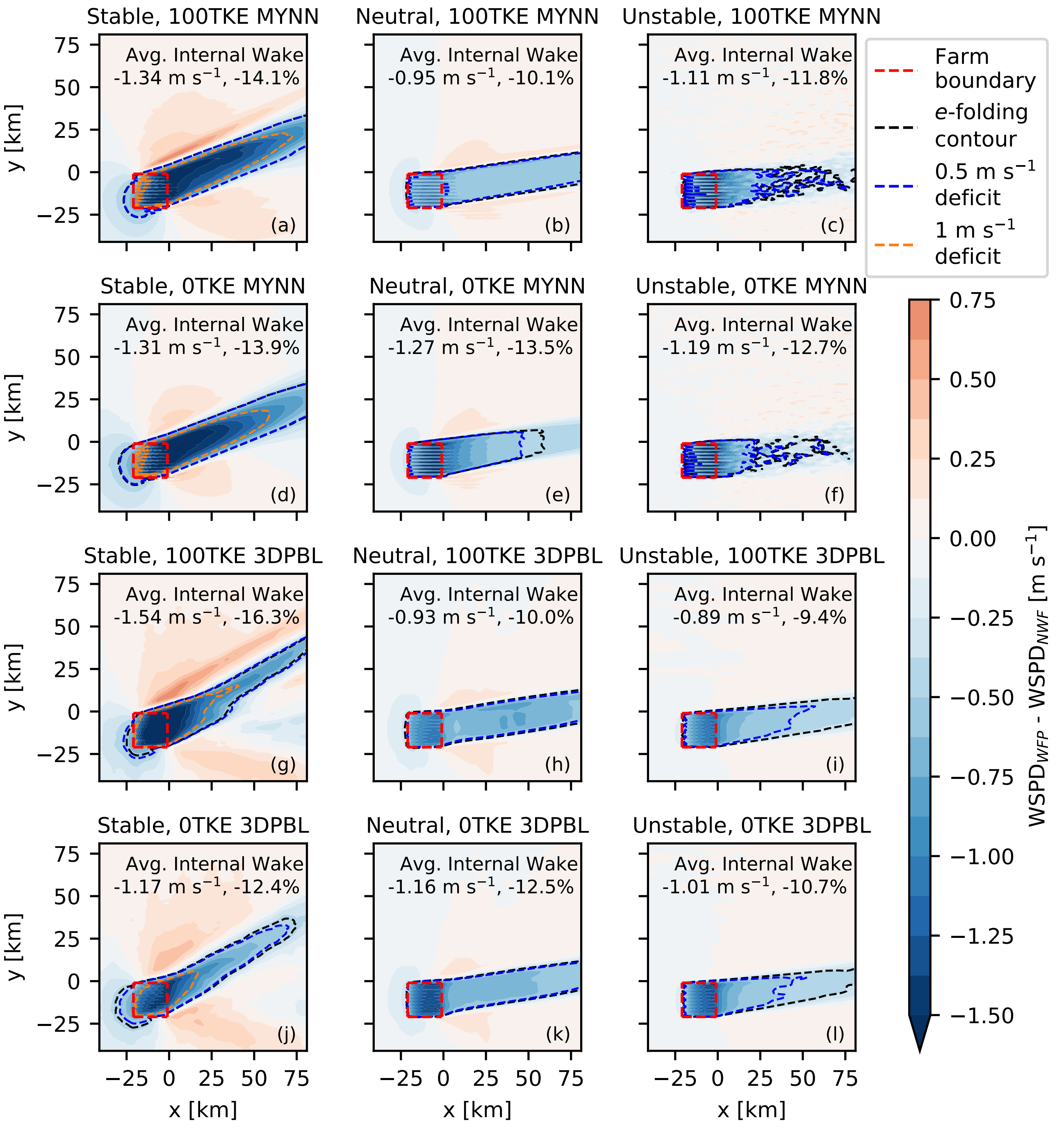

Figure 3. Hub-height wind speed deficits in varying stabilities (left-right) and PBL configurations (up-down). Average hub-height wind speed deficits inside the plant are noted—both in absolute magnitude as well as a percentage relative to the NWF winds. The 1 m s^{-1} deficit contour is highlighted only for the stable simulations, as it obscures internal wakes for other stabilities. Wakes are rotated from the U-geostrophic wind due to the combination of friction and the Coriolis force.

m s^{-1} / ~~-2.5~~ -2.2 percentage points [pp] (in the stable 100TKE simulations) to +~~0.24~~ 0.22 m s^{-1} / +2.4 pp (in the unstable 100TKE simulations). This large spread induces significantly different predictions of power production (Sec. 3.6).

While these simulations show that ~~internal wakes~~ wakes within the plant *can* substantially differ, they do not reveal any obvious patterns of how they *will* differ across conditions. At times, the MYNN simulations produce stronger ~~internal wakes~~ wakes internally than the 3DPBL, whereas MYNN wakes are weaker at other times. Sometimes, turning explicit TKE addition off decreases the internal wake magnitude (e.g., stable conditions), whereas other times it increases internal wake strength (e.g., neutral and unstable conditions). Sometimes MYNN internal wake strength changes more substantially when explicit TKE addition is turned off (e.g., neutral and unstable conditions), whereas 3DPBL internal wake strength changes more substantially at other times (e.g. stable conditions). Thus, this variability within the idealized runs suggests that real-world case studies should be ~~run that are~~ tailored to a specific region and turbine configuration.

In addition to characterizing ~~internal wakes~~ wakes within the extent of the plant, we analyze ~~external wakes~~ wakes outside the plant. There is no singular standard approach that is used to characterize ~~external wakes~~ wakes external to a plant (Fischereit et al., 2021), so we adopt three approaches: by identifying the contours of the 1 m s^{-1} deficit, by identifying the contours of the 0.5 m s^{-1} deficit, and by identifying the e-folding contour. We calculate the e-folding contour as $1/e$ times the average internal wake strength, or about 36% (Fitch et al., 2012), and as such, this uses a relative metric whereas the other contours use an absolute metric. We employ the 1 m s^{-1} contour to highlight regions of strong external ~~wakes~~ waking and the 0.5 m s^{-1} contour to emphasize moderate external ~~wakes~~waking. We only include the 1 m s^{-1} deficit contour in the stable simulations, as this contour obscures internal wakes in the neutral and unstable simulations. We note that choosing one definition versus the other can lead to definitions of ~~external~~ wake lengths that differ by tens of kilometers.

~~External wake behavior~~ Wake behavior outside the plant varies just as much as ~~internal wake behavior~~ it did inside the plant (Fig. 3). The most severe ~~external~~ waking, demarcated by the 1 m s^{-1} deficit contour, varies with stability as expected from previous work, with the strongest wakes in stable conditions. The 1 m s^{-1} contours extend the furthest in stable conditions, whereas they travel at most about ten km downwind in neutral ~~in stable~~ and unstable conditions. We note that MYNN predicts ~~external~~ wakes that are tens of km longer than the 3DPBL does in stable conditions. The addition of explicit TKE consistently increases the ~~external~~ wake length, regardless of what metric is used to define the ~~external~~ boundary of the wake. This increase is seen most clearly in the neutral MYNN simulations (Fig. 3b,e), where ~~external~~ wake length grows by dozens of kilometers. All stable and all unstable simulations show a growth in ~~external~~ wake lengths, roughly on the scale of about 10 km. We also note that neither MYNN nor the 3DPBL show consistently longer ~~external~~ wake lengths across all stabilities. Stability impacts on moderate intensity wakes (either the 0.5 m s^{-1} contour or the e-folding contour) are more varied. For example, the e-folding contour is smaller in the stable 3DPBL simulations than in the neutral 3DPBL or unstable 3DPBL simulations.

We briefly digress from the discussion on wakes to discuss two effects that are secondary to the primary analysis of this study: upwind blockage and flow acceleration. Upwind blockage (Schneemann et al., 2021; Sanchez Gomez et al., 2021) occurs in some of the idealized simulations. Blockage is strongest in the stable conditions, where 0.5 m s^{-1} deficits extend 5 km–10 km upwind of the plant. Under neutral conditions, blockage of up to 0.25 m s^{-1} extends 3 km–5 km upwind of the plant. Blockage does not appear in the unstable simulations. In general, blockage here is a function of stability but not

PBL scheme or TKE addition. Tangential flow accelerations, similar to the speed-ups seen by Nygaard and Hansen (2016), can be observed adjacent to the wakes. The hub-height wind acceleration neighboring the wakes is also a function of stability (strongest in stable conditions, weakest in unstable conditions), but it also varies with TKE addition (stronger acceleration when TKE addition in turned on).

3.3 Vertical Structure of Wind Speed Deficits

While hub-height winds are particularly important to quantify, it is also helpful to characterize wakes over the vertical extent of the rotor disk. We calculate the wind speed deficit averaged across the y-extent (predominantly crosswind) of the plant for each simulation (Fig. 4). Just as the top-down view (Fig. 3) of wind speed deficits suggested, the stable simulations produce the strongest wind speed deficit profiles. Blockage is also visible upwind of the plant in stable conditions. In contrast, the neutral and unstable simulations produce wind speed deficits that are relatively similar to one another. The stronger stable wind speed deficits occur, in part, because of the shallow capping inversion that sits just above the top of the rotor disk. The wakes in the neutral and unstable simulations are able to mix with stronger ambient winds above the plant, thereby eroding the wake, whereas this behavior is not possible in the stable simulations.

The side-view of wind speed deficits show that vertical mixing of wind speed deficits increases when explicit TKE generation is turned on. This behavior consistently occurs across all simulations. The wind speed deficits above the wind plants are stronger in the neutral 100TKE simulations and in the unstable 100TKE simulations than in their counterparts with 0TKE. As a result, the neutral and unstable 0TKE simulations have stronger maximum wind speed deficits within the rotor disk than their 100TKE counterparts. For example, the neutral 100TKE MYNN simulation shows a maximum wind speed deficit of 1.125 m s^{-1} within the rotor disk whereas the neutral 0TKE MYNN has a maximum deficit of 1.625 m s^{-1}. While the shallow capping inversion in the stable simulations obscures the effects of explicit TKE addition above the plant, the TKE effects can be seen below the plant. When explicit TKE addition is turned on in the stable simulations, flow acceleration occurs below the rotor disk, but this acceleration does not occur when TKE addition is turned off. We note that acceleration under the rotor disk was observed in Bodini et al. (2021b) but not in Archer et al. (2019). Correlating with the presence of flow acceleration below the rotor disk, the stable 100TKE simulations show stronger wind speed deficits within the rotor disk than the stable 0TKE simulations.

Finally, the side-view of wind speed deficits also shows that the choice of PBL scheme can be important. The most pronounced differences between PBL schemes occur in stable conditions. For example, the wind speed deficit in the 0TKE 3DPBL simulation stays stronger than 2 m s^{-1} for 50 km downwind of the plant, whereas the wake recovers more quickly in the 0TKE MYNN simulation.

3.4 Difference in Momentum Tendencies

In large part, the two PBL schemes produce different wind speed deficits in their wakes because the schemes parameterize turbulent fluxes differently, as we visualize here. The u and v components of wind speed are modified by mechanisms such as advection of the mean wind, the Coriolis force, and the divergence of the turbulent momentum fluxes (Stull, 1988, Eqn. 3.4.3c). We expect all these terms, aside from the divergence of turbulent momentum fluxes, to be similar for both MYNN and the

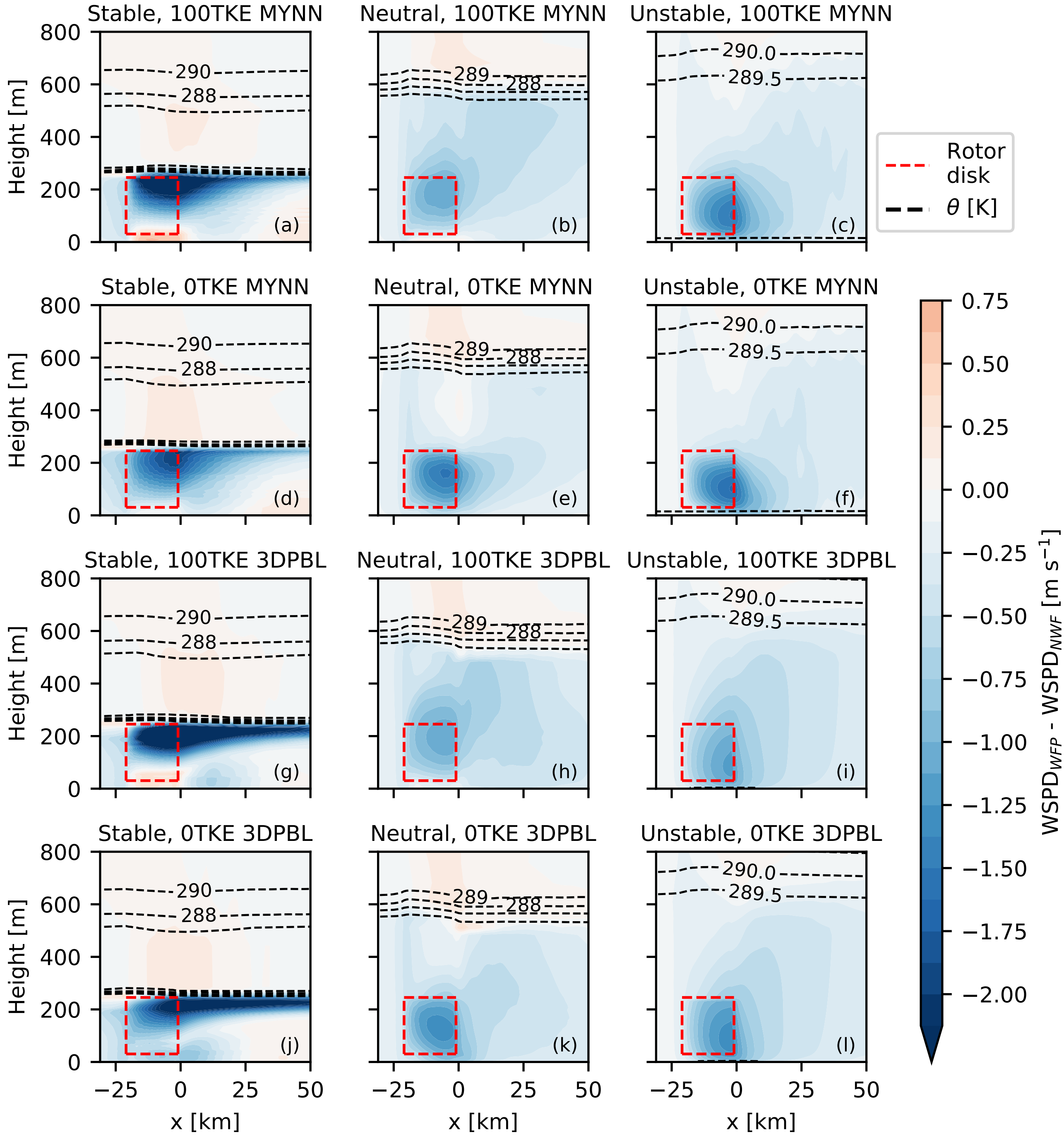

Figure 4. Side view of horizontally averaged wind speed deficits in varying stability conditions (left-right) and PBL configurations (up-down). Horizontal averaging was taken between the north-most and south-most turbines. The height of the ABL is conveyed with θ contours.

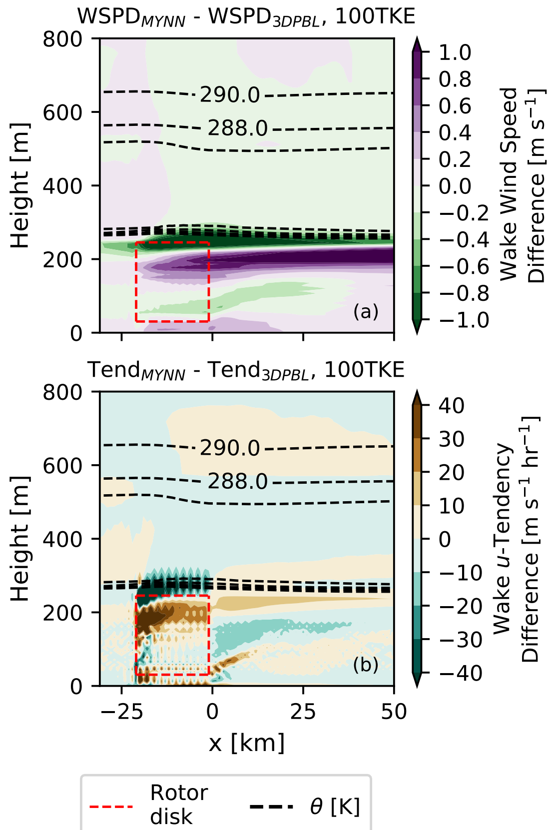

Figure 5. (a) Side view of the difference in wind speed deficits in the stable 100TKE simulations. For example, Figure 5a was calculated as ~~panel~~ the difference between the results in panels Figs. 4a–4g. (b) The u-tendency deficits in the 100TKE simulations are calculated ~~in~~ using a similar ~~manner~~procedure involving tendencies. Potential temperature θ values that have been averaged over the y-extent of the plant are taken from the MYNN simulations.

3DPBL, as the NWF wind speeds are similar but two PBL schemes parameterize momentum fluxes uniquely. We calculate the u-tendency due to the turbulent flux divergence as the vertical derivative of $\overline{u'w'}$, neglecting the horizontal components of flux divergence because they are significantly smaller in the 3DPBL than $\overline{u'w'}$, and they are not computed in the MYNN parameterization. We also omit visualizations of v-tendency because they are substantially smaller than the u-tendency in these idealized simulations forced with a u geostrophic wind. We investigate the relationship of wind speeds and turbulent fluxes between the two PBL schemes in the stable 100TKE simulations by comparing two fields in the wakes—the wind speed deficits and the turbulent flux divergence u-tendency "deficits" (Fig. 5). The u-tendency deficits are defined as tendencies in the turbine-free simulations subtracted from tendencies in the turbine-including simulations.

The differences in tendency deficits between the two PBL schemes drive the differences in the wind speed wakes. As winds advect primarily along the x-direction, wind speed magnitudes are modified by the tendency. For example, the u-tendency is more negative for MYNN above the rotor disk. Correspondingly, the MYNN wind speed deficits in this region as well as downwind of this region are more negative. The same pattern of behavior occurs in the upper half of the rotor disk, where the u-tendency for the 3DPBL is more negative and therefore the 3DPBL wind speed deficits are more negative. Thus, the modeled wind speed deficits in the wake of a plant depend on how the PBL scheme parameterizes turbulent momentum fluxes.

3.5 Total TKE

Just as wind speed deficits are sensitive to the choice of PBL scheme, TKE associated with the wind plant also varies as a function of PBL scheme, stability, and explicit TKE generation (Fig. 6). The WFP induces changes in TKE, and the changes are primarily constrained within the horizontal extent of the plant and tend to not advect far downwind. In contrast, the real onshore WRF WFP simulations of Mangara et al. (2019), saw substantial TKE changes 20 km–30 km downwind. The 100TKE simulations produce substantially more TKE than the 0TKE simulations, as would be expected. The 100TKE 3DPBL simulations also consistently predict stronger levels of additional TKE than their MYNN counterparts. For example, the maximum added TKE in the 100TKE stable simulations was ~~1.250~~ 1.375 $\mathrm{m^2\ s^{-2}}$ for the 3DPBL and 0.750 $\mathrm{m^2\ s^{-2}}$ for MYNN.

The behavior of the 0TKE simulations was more varied. In neutral conditions, both the 0TKE MYNN and 0TKE 3DPBL simulations create a moderate amount of shear-generated TKE at the top of the rotor disk. However in unstable conditions, the 0TKE 3DPBL simulation shows shear-generated TKE whereas the 0TKE MYNN simulation does not. In stable conditions, the 0TKE simulations lack shear-generated TKE at the top of the rotor disk due to the low capping inversion. However, the stable 0TKE 3DPBL turbine-including simulation actually has less TKE than the turbine-free simulation. The LLJ in the turbine-free simulation exhibits strong wind speed shear, and the presence of the wind farm reduces that shear, leading to this behavior.

3.6 Power

Power production and power losses due to internal waking change with PBL scheme (Fig. 7). We calculate the capacity factor for each turbine, the average capacity factor of the plant, and the average power deficit due to internal wakes with reference to the NWF hub-height wind speed. Capacity factor is defined as the ratio of actual power output relative to the maximum possible power output. Across all simulations, the average capacity factor for the plant ranged between 39.5% and ~~51.2~~53.8%. Capacity factor losses due to internal wakes ranged between ~~21.0~~ 16.7 pp and 31.6 pp.

Power production in the idealized simulation varies with the simulation parameters. As discussed earlier (Sec. 3.2), when explicit TKE addition is turned off, hub-height wind speed deficits can either increase or decrease. Accordingly, turning off explicit TKE generation can either grow or shrink the capacity factor. Turning off explicit TKE generation changes internal wake losses ~~by between -7.4~~ to capacity factor by between -6.9 pp (in the stable 3DPBL) and 5.2 pp (in neutral MYNN). Changing from one PBL scheme to another results in wake loss shifts of a similar magnitude—switching from MYNN to the 3DPBL changes internal wake losses by between ~~-0.8~~ -3.4 pp (in stable 100TKE simulations) and ~~8.9~~ -9.6 pp (in unstable ~~0TKE~~ 100TKE simulations). Thus, these simulations emphasize the critical role of PBL scheme on power production.

In the end, these power calculations emphasize that the behavior of modeled power losses are complicated, even in a simple idealized environment. We stress that these idealized simulations have been carried out for one set of hub-height winds in one

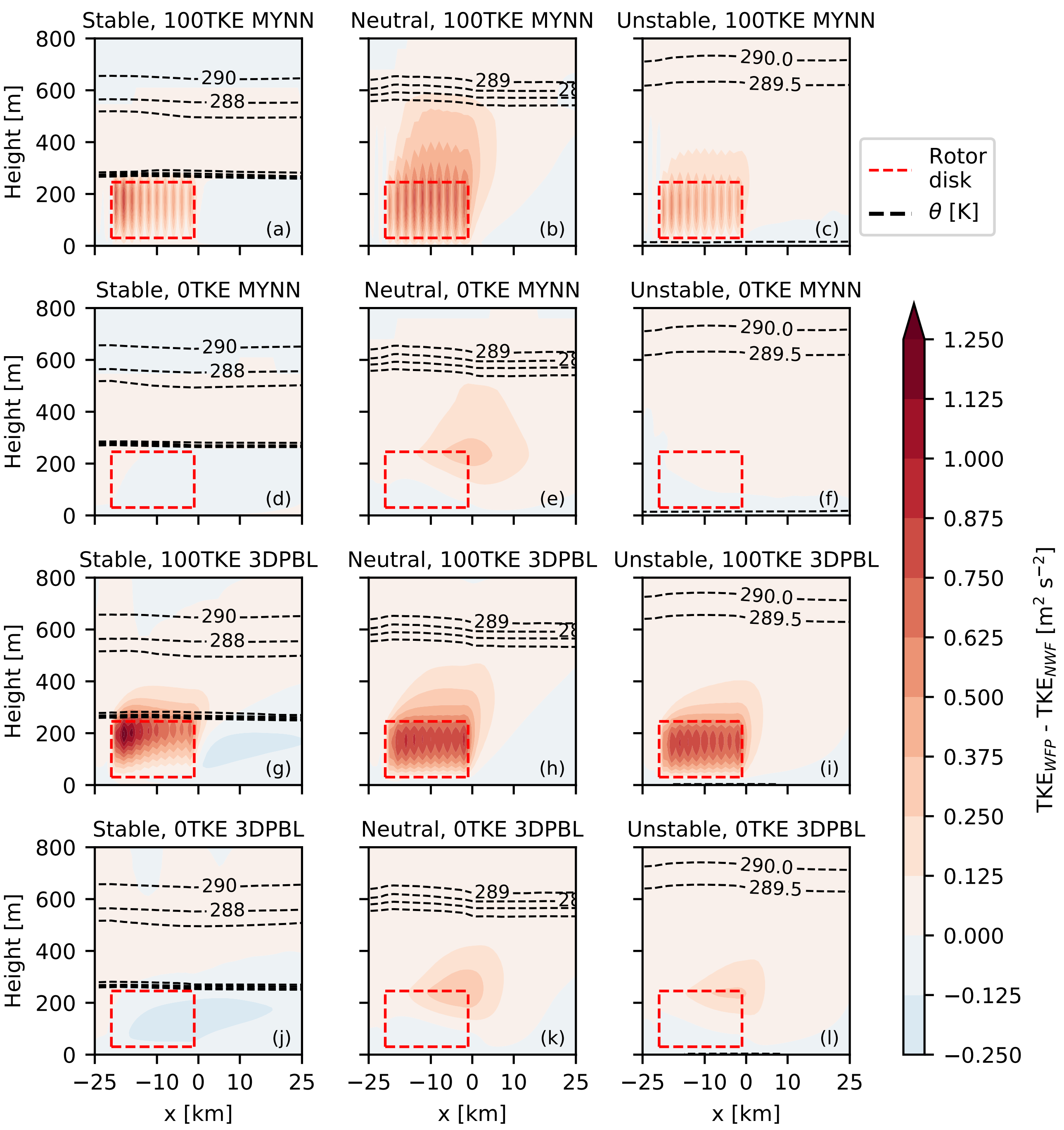

Figure 6. ~~Side view of horizontally averaged~~ Same as Fig. 4, but for TKE in varying stabilities (left-right) and PBL configurations (up-down). The height of the ABL is visualized in the stable and neutral simulations with θ contours.

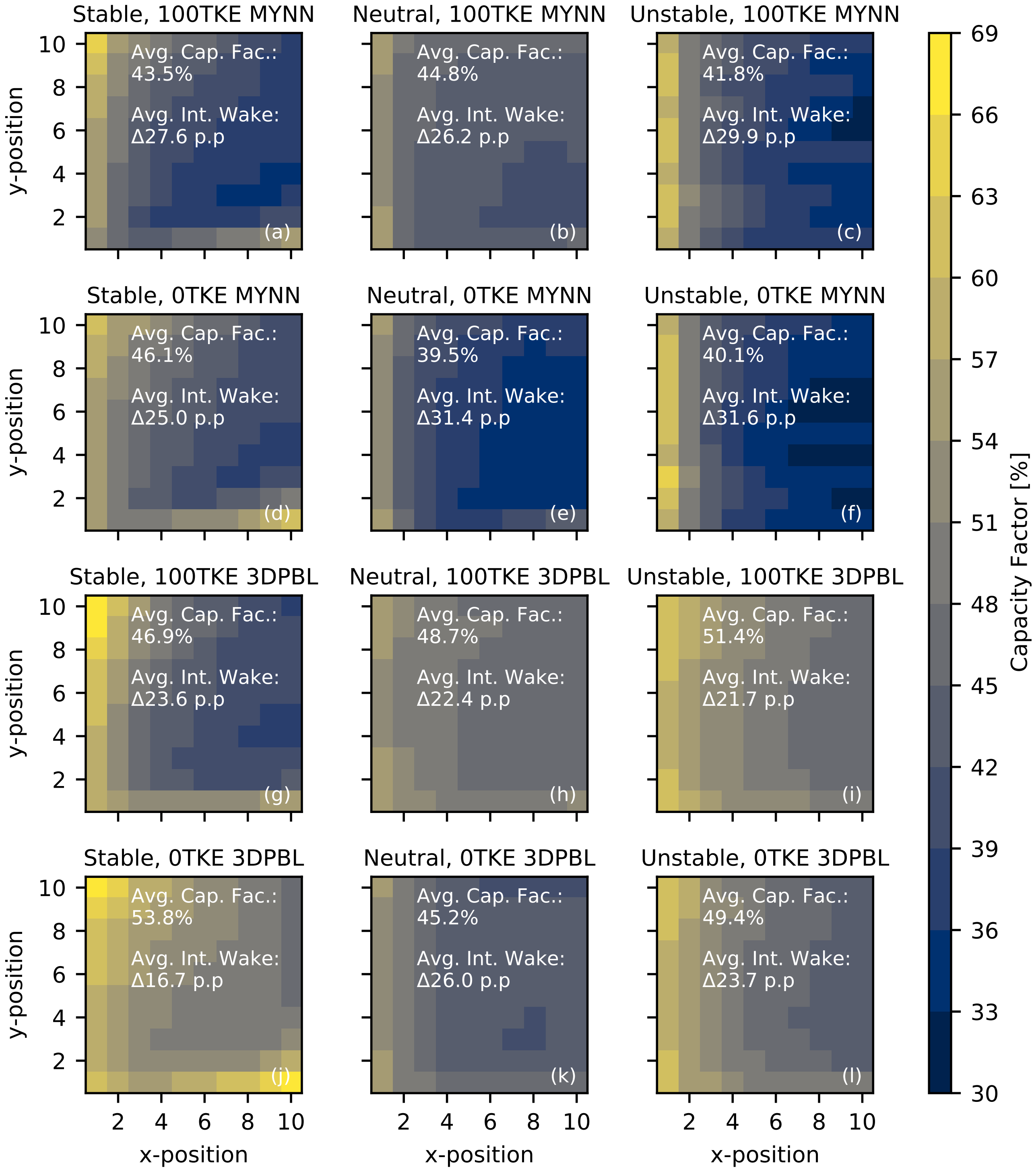

Figure 7. Heat maps of capacity factor for each turbine, based on the turbine's position in the plant. The average capacity factor and internal wake strength are noted for each simulation.

part of the power curve under pseudo-steady conditions. To better predict the cumulative non-linear interactions of the effects of these parameters on losses at a real-world location, ~~we simulate a month-long case study in the U.S. mid-Atlantic coast.~~ it is critical to run real simulations.

4 ~~Results: Mid-Atlantic Case Study~~

~~In this section, we compare wind speed deficits in wakes produced with MYNN and the 3DPBL in August 2020 in the mid-Atlantic. As described in Sec. **??**, we run three categories of simulations—NWF, Vineyard Wind 1 only, and all the lease areas. This set of simulationsallows us to differentiate between internal and external waking at the Vineyard Wind 1 site.~~

3.1 ~~Turbine-Free Winds~~

~~Before analyzing wake effects in the mid-Atlantic, we first examine winds in turbine-free simulations. Specifically, we calculate average profiles at the middle of Vineyard Wind 1. We classify each 5-minute interval WRF output as stable, neutral, or unstable. While a number of metrics can be used to classify atmospheric stability (e.g., bulk Richardson number, Obukhov length), we use WRF-predicted surface heat fluxes at the Vineyard Wind 1 centroid to facilitate comparison to the idealized simulations. We define stable conditions as having a heat flux less than -5 W m^{-2}, unstable conditions as having a heat flux greater than 5 W m^{-2}, and neutral conditions as in between. We designate these thresholds so they overlap with the stability metrics used in the idealized simulations. We emphasize that offshore heat fluxes in this domain are significantly weaker than typical heat fluxes observed on land. As such, while we refer to atmospheric states as "stable" and "unstable" in this offshore environment, these states can resemble the onshore atmosphere under near-neutral stratification. MYNN and the 3DPBL spend a similar percentage of the month under stable conditions (35% and 33%, respectively), whereas MYNN shows more frequent neutral conditions than the 3DPBL (50% versus 40%) and, conversely, MYNN shows less frequent unstable conditions than the 3DPBL (15% versus 27%).~~

~~Averaged wind speed profiles at the Vineyard Wind 1 centroid for August 2020 simulations in (a) stable (surface heat flux < -5 W m^{-2}), (b) neutral (-5 W m^{-2} < surface heat flux < 5 W m^{-2}), and (c) unstable (surface heat flux > 5 W m^{-2}) conditions. Average hub-height wind speeds are noted.~~

~~The average NWF wind speed profiles at Vineyard Wind 1 differ from the idealized wind speed profiles (Fig. **??**). Whereas the idealized simulations force the hub-height wind speeds to match, the mid-Atlantic simulations share large-scale forcing but manifest different hub-height wind speeds due to the PBL schemes. Stable profiles at Vineyard Wind 1 have the fastest wind speeds, and MYNN has a faster average hub-height wind speed than the 3DPBL (12.19 m s^{-1} versus 11.21 m s^{-1}, respectively). The unstable simulations have the second-fastest wind speeds, where MYNN hub-height wind speeds are 9.78 m s^{-1} and 3DPBL hub-height wind speeds are 7.69 m s^{-1}. Thus, simply based off the NWF profiles, we expect MYNN to predict larger power output in stable and unstable conditions than the 3DPBL. The two PBL schemes produce similar weak wind speed profiles in neutral conditions.~~

~~Wind roses at the Vineyard Wind 1 centroid showing the distribution of wind speed (binned by power curve region) with wind direction.~~

~~As wind directions vary in these simulations, we also characterize the distribution of hub-height NWF wind directions and wind speeds using a wind rose at the Vineyard Wind centroid (Fig. **??**). Under stable and neutral conditions, winds are predominantly out of the southwest, whereas under unstable conditions, they are out of the northeast and presumably influenced by land, the island of Martha's Vineyard. Thus, the wakes under unstable conditions extend to the southwest, opposite to those under neutral and stable conditions, which extend to the northeast. In all three stability conditions, the distribution of wind directions is fairly narrow, which facilitates the appearance of wakes in time-averaged visualizations. MYNN shows a greater prevalence of winds at rated power (Region III) under stable and unstable conditions. In neutral conditions, both MYNN and 3DPBL winds are predominantly in Region II; therefore, we expect a smaller wind resource (and larger wake effects on power production) in this stability condition.~~

3.1 ~~Average Hub-Height Wind Speed Deficits~~

~~Averaged hub-height wind speed deficits in varying stabilities (left-right) and PBL schemes (up-down) at Vineyard Wind 1. Rows 1 and 3 (a, b, c and g, h, i, respectively) visualize wind speed deficits relative to their respective NWF counterparts at Vineyard Wind 1 only, whereas rows 2 (d, e, f) and 4 (j, k, l) show deficits resulting from all neighboring lease areas. Average hub-height wind speed deficits inside Vineyard Wind 1 are noted. The wind speed deficit percentage is calculated with respect to the NWF Vineyard Wind 1 average wind speed. The line segment used to quantify external wake length is shown in panels (a) and (g).~~

~~We calculate the average hub-height wind speed deficits by stability and turbine construction scenario in the mid-Atlantic (Fig. **??**). We time average the hub-height wind speeds in the NWF, VW-ONLY, and LEASE simulations, categorizing the stability of each 5-min period based on heat fluxes at the centroid of the NWF Vineyard Wind simulations and using the same timestamps for all three wind turbine cases for each PBL scheme. The distribution of wind direction is narrow in each stability and, as such, we do not additionally filter by wind direction in the wake analysis as might be done at a site with more variable wind directions.~~

~~The mid-Atlantic simulations show that NWF wind speed plays a clear role in dictating internal wake strength (Fig. **??**a–c,g–i). MYNN has faster NWF winds in stable and unstable conditions in the 3DPBL. Correspondingly, MYNN predicts stronger internal wake strengths than the 3DPBL in these stabilities. Likewise, the two PBL schemes predict similar NWF wind speed profiles in neutral conditions, and as such, they predict similar internal wake losses. Thus, while the idealized simulations showed that MYNN and the 3DPBL can generate different wakes when presented with the same hub-height wind speeds, the realistic simulations demonstrate that, additionally, wakes will vary across PBL scheme simply because they predict different hub-height wind speeds. When comparing the two sources of discrepancies (different momentum recovery parameterizations versus different hub-height wind speeds), it appears that the differing hub-height wind speeds more strongly impact internal wakes in the mid-Atlantic.~~

~~Stability also clearly impacts internal wake strength. For both PBL schemes, average NWF wind speed profiles are substantially faster in unstable conditions than in neutral conditions. However, the unstable internal wakes are only 0.1–0.2 m s^{-1} stronger in than under neutral conditions. Thus, wakes erode relatively more quickly in the more turbulent unstable conditions than in neutral conditions, as demonstrated in the idealized simulations (Fig. 3).~~

~~External wake propagation is particularly sensitive to stability and only weakly sensitive to the PBL scheme choice (Fig. **??**d–f,j–l). For simplicity's sake, we characterize external wake propagation in the mid-Atlantic with the 0.5 m s^{-1} contour. As expected, external wakes propagate furthest under stable conditions, and the two PBL schemes predict different lengths. In the stable VW-ONLY cases, they propagate 51 km east of the easternmost point in Vineyard Wind with MYNN and 38 km east with the 3DPBL (Fig. **??**a, g). In the LEASE cases, these external wakes grow in size, although a characteristic length is more difficult to quantify due to their irregular shape.~~

~~Additionally, we quantify the impact of external wakes on hub-height wind speed deficits by focusing on wind speed deficits inside Vineyard Wind 1. We calculate the monthly averaged external wake effect as the average internal wake magnitude in the VW-ONLY simulations subtracted from the perceived internal wake at Vineyard Wind in the LEASE simulations (e.g., Fig. **??**a subtracted from Fig. **??**d). Unsurprisingly, the largest external wake effects occur during stable conditions. MYNN has a stronger external wake effect (0.78 m s^{-1} or 6.4 pp) than the 3DPBL (0.56 m s^{-1} or 5 pp) in these conditions.~~

3.1 ~~Impact on Power Production~~

~~The spatial distribution of average capacity factors at Vineyard Wind 1, binned by stability. Four colormaps are used due to the spread of values by stability and PBL scheme—one for stable simulations, one for neutral simulations, one for unstable MYNN simulations, and one for unstable 3DPBL simulations.~~

~~Power production at Vineyard Wind 1 in the VW-ONLY simulations varies for each of the stability conditions (Fig. **??**a–c, g–i) and PBL schemes. We calculate monthly averaged capacity factors for each of the grid cells within the plant. While wakes are strongest under stable conditions, power production is also largest under stable conditions due to the faster wind speeds. Even though MYNN predicted stronger internal waking, MYNN simulations predict a higher capacity factor than the 3DPBL (64.3% versus 59.7%). Thus, the power gain from the substantially stronger NWF MYNN wind speeds overcomes the power decrease from the marginally stronger wakes. Power production is smallest under neutral conditions where winds are weakest, and the two PBL schemes predict similar capacity factors, owing to the similar NWF profiles. The largest discrepancy in capacity factor occurs under unstable conditions. MYNN's average unstable capacity factor (56.1%) is much larger than the 3DPBL's (38.2%), correlating with MYNN's faster NWF winds. This large discrepancy stems from the differences in wind speed distributions (Fig. **??**c, f).~~

~~While the two PBL schemes can predict substantially different capacity factors, they predict similar power losses associated with internal wakes. We calculate the expected unwaked power production in the idealized simulations by convolving the time-varying hub-height wind speeds with the power curve, and we calculate internal wake power loss with reference to this value. During stable conditions, MYNN predicts only slightly stronger losses than the 3DPBL (26.2 pp loss versus 24.9 pp loss). During unstable conditions, we see the same general behavior—average MYNN losses are 12.4 pp and average 3DPBL~~

~~losses are 10.3 pp. Even though winds were much weaker overall under neutral conditions, we also see an approximate 1-pp difference in power loss.~~

~~As was the case for internal internal losses, MYNN and the 3DPBL predict similar external wake losses (Fig. **??**d–f, j–l). Under neutral conditions, external wakes further decrease capacity factors by 2.0 pp regardless of PBL scheme. External wakes in unstable conditions reduce MYNN's average capacity factor by 3.3 pp and the 3DPBL's average capacity factor by 3.6 pp. The two PBL schemes disagree most substantially in stable conditions, for which MYNN shows an 8.1 pp capacity factor decrease whereas the 3DPBL only shows a 5.9 pp decrease. In summary, the different PBL schemes disagree on external wake power losses by 0.3 pp–2.2 pp across the different stabilities.~~

~~Finally, we demonstrate the importance of PBL scheme choice by taking a macro-view of the mid-Atlantic simulations and calculating average capacity factors across the entire month, irrespective of stability distributions. At Vineyard Wind 1, in the VW-ONLY simulations, MYNN's month-long average capacity factor is 38.5%; the 3DPBL's average capacity factor is 36.3%. When external waking is considered, MYNN shows a capacity factor of 36.0% and the 3DPBL shows a capacity factor of 33.2% at Vineyard Wind 1. When all lease areas in the LEASE simulations are considered, the capacity factor is 36.0% for MYNN and 33.2% for the 3DPBL. In summary, across all scenarios, the 3DPBL predicts capacity factors that are 1.6 pp–2.8 pp less than in MYNN—or about 4.7%–7.8% less total power generated.~~

3.1 ~~Time-Varying Wake Impacts and Power Production~~

~~(a) A week of hub-height NWF wind speeds at the Vineyard Wind 1 centroid. (b) Wind directions at the same location. (c) Spatially averaged capacity factor at Vineyard Wind 1 in the VW-ONLY simulation. (d) Internal waking, as characterized by differences in spatially averaged capacity factors between the NWF and VW-ONLY simulations. (e) External waking, as characterized by differences in spatially averaged capacity factors between the VW-ONLY and LEASE simulations. Periods with significant external waking are highlighted in red in panels (b) and (e).~~

~~The key role that NWF wind speed plays on power production emerges clearly in time series analysis of NWF hub-height winds, capacity factor, and wake effects for one week of the simulation (Fig. **??**). In general, when NWF hub-height winds at the Vineyard Wind 1 centroid are stronger for a given PBL scheme (Fig. **??**a), that PBL scheme also produces more instantaneous power (Fig.**??**c). This power production difference is particularly true when NWF wind speeds are in the vicinity of the rated wind speed (between Region II and Region III), as occurs on August 23. This pattern also persists when winds are weaker (as they are between August 24–25), although it is less prominent because the wakes are also weaker. Differences in predicted wind speed are less important when NWF winds exceed the rated speed (as on August 26), as internal wakes in the VW-ONLY simulation do not reduce power output. Even then, external wakes can further weaken winds inside Vineyard Wind and reduce power output, as they momentarily do on August 26. Regarding external wakes, even minor differences in NWF wind direction between PBL schemes ($< 5°$, Fig. **??**b) can produce instantaneous external wake effects that differ by a dozen pp or greater (Fig. **??**e), as occurs on August 23.~~

~~While faster wind speeds tend to lead to a larger capacity factor for a given PBL, faster wind speeds do not necessarily cause stronger internal or external waking. During the first red-highlighted period of Fig. **??**, MYNN has faster NWF wind~~

~~speeds but weaker internal waking. This disparity could be explained by subtle differences in NWF wind direction, significant spatial variability of wind directions within Vineyard Wind 1 (rendering the single-point measurement of wind direction less informative), or differences in mixing for each PBL scheme, among other factors.~~

~~In the end, these timeseries figures show that the two PBL schemes can predict capacity factors that differ by dozen of pp in a given moment. Thus, when seeking to characterize power production uncertainty, it may be even more beneficial to vary PBL schemes for short-term wind forecasts than for long-term wind resource assessments.~~

4 Conclusions

In this analysis, we studied the sensitivity of NWP-modeled mesoscale wakes to two PBL schemes: the widely-used MYNN and the recently introduced NCAR 3DPBL. While prior studies have showed that NWP-modeled wind resource in turbine-free simulations can significantly vary with PBL scheme, the same sensitivity has not yet been studied in simulations with explicitly resolved turbines. We integrated the NCAR 3DPBL with the Fitch wind farm parameterization and then examined modeled wake sensitivity ~~in two contexts. First, we~~ through a series of simulations. We simulated pseudo-steady idealized stable, neutral, and unstable environments with hub-height wind speeds of approximately 9.35 m s^{-1}. In this context, we also examined wake sensitivity to the amount of explicitly added TKE from the Fitch wind farm parameterization. ~~Second, we ran a month-long case study in the mid-Atlantic United States, centered on the Vineyard Wind 1 wind plant.~~

We summarize key findings from this analysis.

- ~~The choice of PBL scheme had a significant impact on power production in the mid-Atlantic. Depending on turbine layout, the 3DPBL predicts that 4.7%–7.8% less power would be generated in the mid-Atlantic relative to MYNN across August 2020. MYNN predicts stronger power output, in large part, because it predicts stronger inflow winds.~~

- ~~While the two PBL schemes produced substantially different capacity factors in the mid-Atlantic, they predicted relatively similar power losses due to internal wakes, differing by only 1–2 percentage points. Average internal losses at Vineyard Wind 1 were about 25.5 ± 0.6 percentage points under stable conditions, 10 ± 0.5 percentage points under neutral conditions, and 11 ± 1 percentage point under unstable conditions. Average losses due to external wakes showed slightly more variability between PBL schemes but, in the end, they further reduced average capacity factors at Vineyard Wind 1 by about 6–8 percentage points under stable conditions, 2 percentage points under neutral conditions, and 3–4 percentage points under unstable conditions.~~

- ~~Correspondingly, wind speed deficits in the mid-Atlantic were similar but distinct across PBL schemes. When characterizing wind speed losses as a percentage of turbine-free winds, the two schemes agreed well. Internal wake losses differed by at most 0.6 percentage points, whereas external wake losses differed by 2.0 percentage points at most. When characterizing wind speed losses in using absolute wind speeds, these differences were larger.~~

- In the idealized simulations, both capacity factor and wake losses were substantially impacted by PBL scheme, the presence or omission of explicit TKE addition, and the stability. Average capacity factors ranged between 39.5~~–51.2~~–53.8% and wakes reduced the average capacity factors by ~~21.0~~16.7–31.6 percentage points.
- Similarly, wind speed deficits were significantly impacted by these factors in the idealized simulations. MYNN predicted ~~internal wakes~~ average wind speed deficits within the extent of the plant that differed from those in the 3DPBL by between ~~-0.24~~ -0.20 m s^{-1} to ~~0.24~~ 0.22 m s^{-1} (or ~~-2.5~~ -2.2 to 2.4 percentage points for relative wake magnitude). Additionally, MYNN predicted strong external wakes that traveled dozens of km longer than the 3DPBL in stable conditions.
- While the magnitude of wind speed deficits typically varied with PBL scheme, an obvious pattern did not emerge. At times, MYNN predicted stronger deficits, whereas sometimes the 3DPBL had stronger deficits. In contrast, wakes consistently grew longer when explicit TKE addition was turned on.

Through our study, ~~we set out~~ begin to address the question "How sensitive are modeled mesoscale wakes to the choice of PBL parameterization?" We find that, indeed, modeled mesoscale wakes can be significantly sensitive to the choice of PBL scheme ~~. Due to this sensitivity~~ in idealized simulations. This suggests that real mesoscale simulations of planned wind plants could also be significantly sensitive to the choice of PBL scheme. Indeed, preliminary offshore simulations in the U.S. mid-Atlantic show that MYNN and the 3DPBL can predict month-long power production that differs by as much as 7.8% (Rybchuk, 2022). Due to the model sensitivity discussed throughout this manuscript, we recommend that future wind energy planning studies that examine mesoscale model sensitivity consider varying the PBL scheme, along with other model inputs that have been established in literature, such as grid resolution, magnitude of explicit TKE addition, and the choice of wind farm parameterization (Fischereit et al., 2021). By better characterizing the uncertainty associated with NWP-modeled wind resource, wind plant developers will be able to take on less risk when developing future wind plants.

Code and data availability. Namelists for all simulations, time-averaged idealized WRF data, WRF code modifications, and analysis notebooks to reproduce all figures can be found on Zenodo (https://doi.org/10.5281/zenodo.5565399). For convenience, much of the same material has also been uploaded to GitHub (https://github.com/rybchuk/wfp-3dpbl-sensitivity).

Author contributions. **Alex Rybchuk**: Methodology, Investigation, Data Curation, Writing – original draft preparation, Writing – review & editing; **Timothy W. Juliano**: Methodology, Software, Writing – review & editing; **Julie K. Lundquist**: Project conception, Funding acquisition, Project administration, Supervision, Writing – review & editing, **David Rosencrans**: Methodology; **Nicola Bodini**: Project administration, Writing – review & editing; **Mike Optis**: Funding acquisition and Project administration.

Competing interests. The authors declare no competing interest are present.

Acknowledgements. We would like to thank Branko Kosović and Pedro Jiménez Munoz for their developments on the NCAR 3DPBL and sharing an early version of the code. We also thank the ~~Pangeo community for their support with "big data" analysis (Odaka et al., 2020), as well as the~~ Python community at large for the development of libraries such as Matplotlib (Hunter, 2007), Numpy (Harris et al., 2020), Xarray (Hoyer and Hamman, 2017), Dask (Rocklin, 2015), Zarr (Miles et al., 2021), Cartopy (Office, 2010), and Python-windrose (Roubeyrie and Celles, 2018). Finally, we would also like to thank the manuscript editor Andrea Hahmann and the two anonymous reviewers. This work was conducted with support from the National Offshore Wind Research and Development Consortium under Agreement No. CRD-19-16351. A portion of the research was performed using computational resources sponsored by the Department of Energy's Office of Energy Efficiency and Renewable Energy and located at the National Renewable Energy Laboratory. This work utilized resources from the University of Colorado Boulder Research Computing Group, which is supported by the National Science Foundation (awards ACI-1532235 and ACI-1532236), the University of Colorado Boulder, and Colorado State University. JKL's and AR's effort was partially supported by the National Science Foundation under CAREER grant AGS-1554055~~. Neither NYSERDA nor OceanTech Services/DNV have reviewed the information contained herein and the opinions in this report do not necessarily reflect those of any of these parties~~.

References

Abkar, M. and Porté-Agel, F.: A New Wind-Farm Parameterization for Large-Scale Atmospheric Models, Journal of Renewable and Sustainable Energy, 7, 013 121, https://doi.org/10.1063/1.4907600, 2015.

Archer, C. L., Colle, B. A., Monache, L. D., Dvorak, M. J., Lundquist, J., Bailey, B. H., Beaucage, P., Churchfield, M. J., Fitch, A. C., Kosovic, B., Lee, S., Moriarty, P. J., Simao, H., Stevens, R. J. A. M., Veron, D., and Zack, J.: Meteorology for Coastal/Offshore Wind Energy in the United States: Recommendations and Research Needs for the Next 10 Years, Bulletin of the American Meteorological Society, 95, 515–519, https://doi.org/10.1175/BAMS-D-13-00108.1, 2014.

Archer, C. L., Wu, S., Vasel-Be-Hagh, A., Brodie, J. F., Delgado, R., St. Pé, A., Oncley, S., and Semmer, S.: The VERTEX Field Campaign: Observations of near-Ground Effects of Wind Turbine Wakes, Journal of Turbulence, 20, 64–92, https://doi.org/10.1080/14685248.2019.1572161, 2019.

Archer, C. L., Wu, S., Ma, Y., and Jiménez, P. A.: Two Corrections for Turbulent Kinetic Energy Generated by Wind Farms in the WRF Model, Monthly Weather Review, 148, 4823–4835, https://doi.org/10.1175/MWR-D-20-0097.1, 2020.

Beiter, P., Musial, W., Duffy, P., Cooperman, A., Shields, M., Heimiller, D., and Optis, M.: The Cost of Floating Offshore Wind Energy in California Between 2019 and 2032, Tech. Rep. NREL/TP-5000-77384, National Renewable Energy Lab. (NREL), Golden, CO (United States), https://doi.org/10.2172/1710181, 2020.

Bodini, N., Hu, W., Optis, M., Cervone, G., and Alessandrini, S.: Assessing Boundary Condition and Parametric Uncertainty in Numerical-Weather-Prediction-Modeled, Long-Term Offshore Wind Speed through Machine Learning and Analog Ensemble, Wind Energy Science, 6, 1363–1377, https://doi.org/10.5194/wes-6-1363-2021, 2021a.

Bodini, N., Lundquist, J. K., and Moriarty, P.: Wind Plants Can Impact Long-Term Local Atmospheric Conditions, Scientific Reports, 11, 22 939, https://doi.org/10.1038/s41598-021-02089-2, 2021b.

BOEM: Renewable Energy GIS Data | Bureau of Ocean Energy Management, https://www.boem.gov/renewable-energy/mapping-and-data/renewable-energy-gis-data, 2020.

Brower, M., Bernadett, D. W., Elsholz, K. V., Filippelli, M. V., Markus, M. J., Taylor, M. A., and Tensen, J.: Wind Resource Assessment: A Practical Guide to Developing a Wind Project, John Wiley & Sons, Incorporated, Somerset, UNITED STATES, 2012.

Carvalho, D., Rocha, A., Gómez-Gesteira, M., and Santos, C.: A Sensitivity Study of the WRF Model in Wind Simulation for an Area of High Wind Energy, Environmental Modelling & Software, 33, 23–34, https://doi.org/10.1016/j.envsoft.2012.01.019, 2012.

Carvalho, D., Rocha, A., Gómez-Gesteira, M., and Silva Santos, C.: Offshore Wind Energy Resource Simulation Forced by Different Reanalyses: Comparison with Observed Data in the Iberian Peninsula, Applied Energy, 134, 57–64, https://doi.org/10.1016/j.apenergy.2014.08.018, 2014.

Donlon, C. J., Martin, M., Stark, J., Roberts-Jones, J., Fiedler, E., and Wimmer, W.: The Operational Sea Surface Temperature and Sea Ice Analysis (OSTIA) System, Remote Sensing of Environment, 116, 140–158, https://doi.org/10.1016/j.rse.2010.10.017, 2012.

Draxl, C., Hahmann, A. N., Peña, A., and Giebel, G.: Evaluating Winds and Vertical Wind Shear from Weather Research and Forecasting Model Forecasts Using Seven Planetary Boundary Layer Schemes, Wind Energy, 17, 39–55, https://doi.org/10.1002/we.1555, 2014.

Fernández-González, S., Martín, M. L., García-Ortega, E., Merino, A., Lorenzana, J., Sánchez, J. L., Valero, F., and Rodrigo, J. S.: Sensitivity Analysis of the WRF Model: Wind-Resource Assessment for Complex Terrain, Journal of Applied Meteorology and Climatology, 57, 733–753, https://doi.org/10.1175/JAMC-D-17-0121.1, 2018.

Fields, M. J. and Sherwin, R.: IEC 61400-15 Working Group Update 1, https://doi.org/10.5281/zenodo.3952712, 2017.

Fischereit, J., Brown, R., Larsén, X. G., Badger, J., and Hawkes, G.: Review of Mesoscale Wind-Farm Parametrizations and Their Applications, Boundary-Layer Meteorology, https://doi.org/10.1007/s10546-021-00652-y, 2021.

Fitch, A. C., Olson, J. B., Lundquist, J. K., Dudhia, J., Gupta, A. K., Michalakes, J., and Barstad, I.: Local and Mesoscale Impacts of Wind Farms as Parameterized in a Mesoscale NWP Model, Monthly Weather Review, 140, 3017–3038, https://doi.org/10.1175/MWR-D-11-00352.1, 2012.

Gupta, T. and Baidya Roy, S.: Recovery Processes in a Large Offshore Wind Farm, Wind Energy Science, 6, 1089–1106, https://doi.org/10.5194/wes-6-1089-2021, 2021.

Hansen, K. S., Barthelmie, R. J., Jensen, L. E., and Sommer, A.: The Impact of Turbulence Intensity and Atmospheric Stability on Power Deficits Due to Wind Turbine Wakes at Horns Rev Wind Farm, Wind Energy, 15, 183–196, https://doi.org/10.1002/we.512, 2012.

Harris, C. R., Millman, K. J., van der Walt, S. J., Gommers, R., Virtanen, P., Cournapeau, D., Wieser, E., Taylor, J., Berg, S., Smith, N. J., Kern, R., Picus, M., Hoyer, S., van Kerkwijk, M. H., Brett, M., Haldane, A., del Río, J. F., Wiebe, M., Peterson, P., Gérard-Marchant, P., Sheppard, K., Reddy, T., Weckesser, W., Abbasi, H., Gohlke, C., and Oliphant, T. E.: Array Programming with NumPy, Nature, 585, 357–362, https://doi.org/10.1038/s41586-020-2649-2, 2020.

Haupt, S. E., Berg, L. K., Decastro, A., Gagne, D. J., Jimenez, P., Juliano, T., Kosovic, B., Quon, E., Shaw, W. J., Churchfield, M. J., Draxl, C., Hawbecker, P., Jonko, A., Kaul, C. M., Mirocha, J. D., and Rai, R. K.: Outcomes of the DOE Workshop on Atmospheric Challenges for the Wind Energy Industry, Tech. Rep. PNNL-30828, Pacific Northwest National Lab. (PNNL), Richland, WA (United States), https://doi.org/10.2172/1762812, 2020.

Hersbach, H., Bell, B., Berrisford, P., Hirahara, S., Horányi, A., Muñoz-Sabater, J., Nicolas, J., Peubey, C., Radu, R., Schepers, D., Simmons, A., Soci, C., Abdalla, S., Abellan, X., Balsamo, G., Bechtold, P., Biavati, G., Bidlot, J., Bonavita, M., De Chiara, G., Dahlgren, P., Dee, D., Diamantakis, M., Dragani, R., Flemming, J., Forbes, R., Fuentes, M., Geer, A., Haimberger, L., Healy, S., Hogan, R. J., Hólm, E., Janisková, M., Keeley, S., Laloyaux, P., Lopez, P., Lupu, C., Radnoti, G., de Rosnay, P., Rozum, I., Vamborg, F., Villaume, S., and Thépaut, J.-N.: The ERA5 Global Reanalysis, Quarterly Journal of the Royal Meteorological Society, 146, 1999–2049, https://doi.org/10.1002/qj.3803, 2020.

Hong, S.-Y., Noh, Y., and Dudhia, J.: A New Vertical Diffusion Package with an Explicit Treatment of Entrainment Processes, Monthly Weather Review, 134, 2318–2341, https://doi.org/10.1175/MWR3199.1, 2006.

Hoyer, S. and Hamman, J.: Xarray: N-D Labeled Arrays and Datasets in Python, Journal of Open Research Software, 5, 10, https://doi.org/10.5334/jors.148, 2017.

Hunter, J. D.: Matplotlib: A 2D Graphics Environment, Computing in Science Engineering, 9, 90–95, https://doi.org/10.1109/MCSE.2007.55, 2007.

Iacono, M. J., Delamere, J. S., Mlawer, E. J., Shephard, M. W., Clough, S. A., and Collins, W. D.: Radiative Forcing by Long-Lived Greenhouse Gases: Calculations with the AER Radiative Transfer Models, Journal of Geophysical Research: Atmospheres, 113, https://doi.org/10.1029/2008JD009944, 2008.

Janjić, Z. I.: The Step-Mountain Eta Coordinate Model: Further Developments of the Convection, Viscous Sublayer, and Turbulence Closure Schemes, Monthly Weather Review, 122, 927–945, https://doi.org/10.1175/1520-0493(1994)122<0927:TSMECM>2.0.CO;2, 1994.

Jiménez, P. A., Dudhia, J., González-Rouco, J. F., Navarro, J., Montávez, J. P., and García-Bustamante, E.: A Revised Scheme for the WRF Surface Layer Formulation, Monthly Weather Review, 140, 898–918, https://doi.org/10.1175/MWR-D-11-00056.1, 2012.

Juliano, T. W., Kosović, B., Jiménez, P. A., Eghdami, M., Haupt, S. E., and Martilli, A.: “Gray Zone” Simulations Using a Three-Dimensional Planetary Boundary Layer Parameterization in the Weather Research and Forecasting Model, Monthly Weather Review, -1, https://doi.org/10.1175/MWR-D-21-0164.1, 2021.

Juliano, T. W., Kosović, B., Jiménez, P. A., Eghdami, M., Haupt, S. E., and Martilli, A.: “Gray Zone” Simulations Using a Three-Dimensional Planetary Boundary Layer Parameterization in the Weather Research and Forecasting Model, Monthly Weather Review, 150, 1585–1619, https://doi.org/10.1175/MWR-D-21-0164.1, 2022.

Kosović, B., Munoz, P. J., Juliano, T. W., Martilli, A., Eghdami, M., Barros, A. P., and Haupt, S. E.: Three-Dimensional Planetary Boundary Layer Parameterization for High-Resolution Mesoscale Simulations, Journal of Physics: Conference Series, 1452, 012 080, https://doi.org/10.1088/1742-6596/1452/1/012080, 2020.

Larsén, X. G. and Fischereit, J.: A Case Study of Wind Farm Effects Using Two Wake Parameterizations in the Weather Research and Forecasting (WRF) Model (V3.7.1) in the Presence of Low-Level Jets, Geoscientific Model Development, 14, 3141–3158, https://doi.org/10.5194/gmd-14-3141-2021, 2021.

Lee, J. C. Y. and Fields, M. J.: An Overview of Wind-Energy-Production Prediction Bias, Losses, and Uncertainties, Wind Energy Science, 6, 311–365, https://doi.org/10.5194/wes-6-311-2021, 2021.

Livingston, H. G. and Lundquist, J. K.: How Many Offshore Wind Turbines Does New England Need?, Meteorological Applications, 27, e1969, https://doi.org/10.1002/met.1969, 2020.

Mangara, R. J., Guo, Z., and Li, S.: Performance of the Wind Farm Parameterization Scheme Coupled with the Weather Research and Forecasting Model under Multiple Resolution Regimes for Simulating an Onshore Wind Farm, Advances in Atmospheric Sciences, 36, 119–132, https://doi.org/10.1007/s00376-018-8028-3, 2019.

Mellor, G. L. and Yamada, T.: A Hierarchy of Turbulence Closure Models for Planetary Boundary Layers, Journal of the Atmospheric Sciences, 31, 1791–1806, https://doi.org/10.1175/1520-0469(1974)031<1791:AHOTCM>2.0.CO;2, 1974.

Mellor, G. L. and Yamada, T.: Development of a Turbulence Closure Model for Geophysical Fluid Problems, Reviews of Geophysics, 20, 851–875, https://doi.org/10.1029/RG020i004p00851, 1982.

Miles, A., jakirkham, Bussonnier, M., Moore, J., Fulton, A., Bourbeau, J., Onalan, T., Hamman, J., Patel, Z., Rocklin, M., de Andrade, E. S., Lee, G. R., Abernathey, R., Bennett, D., Durant, M., Schut, V., dussin, r., Barnes, C., Williams, B., Noyes, C., shikharsg, Jelenak, A., Banihirwe, A., Baddeley, D., Younkin, E., Sakkis, G., Hunt-Isaak, I., Funke, J., and Kelleher, J.: Zarr-Developers/Zarr-Python:, Zenodo, https://doi.org/10.5281/zenodo.5579625, 2021.

Nakanishi, M. and Niino, H.: Development of an Improved Turbulence Closure Model for the Atmospheric Boundary Layer, Journal of the Meteorological Society of Japan. Ser. II, 87, 895–912, https://doi.org/10.2151/jmsj.87.895, 2009.

NREL: US Offshore Wind Resource Data for 2000-2019 [Data Set], https://doi.org/10.25984/1821404, 2020.

Nygaard, N. G. and Hansen, S. D.: Wake Effects between Two Neighbouring Wind Farms, Journal of Physics: Conference Series, 753, 032 020, https://doi.org/10.1088/1742-6596/753/3/032020, 2016.

Odaka, T. E., Banihirwe, A., Eynard-Bontemps, G., Ponte, A., Maze, G., Paul, K., Baker, J., and Abernathey, R.: The Pangeo Ecosystem: Interactive Computing Tools for the Geosciences: Benchmarking on HPC, in: Tools and Techniques for High Performance Computing, edited by Juckeland, G. and Chandrasekaran, S., Communications in Computer and Information Science, pp. 190–204, Springer International Publishing, Cham, https://doi.org/10.1007/978-3-030-44728-1_12, 2020.

Office, M.: Cartopy: A Cartographic Python Library with a Matplotlib Interface, 2010.

Olsen, B. T., Hahmann, A. N., Sempreviva, A. M., Badger, J., and Jørgensen, H. E.: An Intercomparison of Mesoscale Models at Simple Sites for Wind Energy Applications, Wind Energy Science, 2, 211–228, https://doi.org/10.5194/wes-2-211-2017, 2017.

Olson, J. B., Kenyon, J. S., Angevine, W. A., Brown, J. M., Pagowski, M., and Sušelj, K.: A Description of the MYNN-EDMF Scheme and the Coupling to Other Components in WRF–ARW, https://doi.org/10.25923/N9WM-BE49, 2019.

Optis, M., Rybchuk, O., Bodini, N., Rossol, M., and Musial, W.: Offshore Wind Resource Assessment for the California Pacific Outer Continental Shelf (2020), Tech. Rep. NREL/TP-5000-77642, National Renewable Energy Lab. (NREL), Golden, CO (United States), https://doi.org/10.2172/1677466, 2020.

Pan, Y. and Archer, C. L.: A Hybrid Wind-Farm Parametrization for Mesoscale and Climate Models, Boundary-Layer Meteorology, 168, 469–495, https://doi.org/10.1007/s10546-018-0351-9, 2018.

Pleim, J. E.: A Combined Local and Nonlocal Closure Model for the Atmospheric Boundary Layer. Part I: Model Description and Testing, Journal of Applied Meteorology and Climatology, 46, 1383–1395, https://doi.org/10.1175/JAM2539.1, 2007.

Pryor, S. C., Shepherd, T. J., Volker, P. J. H., Hahmann, A. N., and Barthelmie, R. J.: “Wind Theft” from Onshore Wind Turbine Arrays: Sensitivity to Wind Farm Parameterization and Resolution, Journal of Applied Meteorology and Climatology, 59, 153–174, https://doi.org/10.1175/JAMC-D-19-0235.1, 2020.

Redfern, S., Olson, J. B., Lundquist, J. K., and Clack, C. T. M.: Incorporation of the Rotor-Equivalent Wind Speed into the Weather Research and Forecasting Model’s Wind Farm Parameterization, Monthly Weather Review, 147, 1029–1046, https://doi.org/10.1175/MWR-D-18-0194.1, 2019.

Rocklin, M.: Dask: Parallel Computation with Blocked Algorithms and Task Scheduling, in: Proceedings of the 14th Python in Science Conference, vol. 130, p. 136, Citeseer, 2015.

Roubeyrie, L. and Celles, S.: Windrose: A Python Matplotlib, Numpy Library to Manage Wind and Pollution Data, Draw Windrose, Journal of Open Source Software, 3, 268, https://doi.org/10.21105/joss.00268, 2018.

Rybchuk, A.: Modeling the Impact of Energy Infrastructure on the Atmospheric Boundary Layer, Ph.D. thesis, 2022.

Sanchez Gomez, M., Lundquist, J. K., Mirocha, J. D., Arthur, R. S., and Muñoz-Esparza, D.: Quantifying Wind Plant Blockage under Stable Atmospheric Conditions, Wind Energy Science Discussions, pp. 1–21, https://doi.org/10.5194/wes-2021-57, 2021.

Schneemann, J., Theuer, F., Rott, A., Dörenkämper, M., and Kühn, M.: Offshore Wind Farm Global Blockage Measured with Scanning Lidar, Wind Energy Science, 6, 521–538, https://doi.org/10.5194/wes-6-521-2021, 2021.

Shaw, W. J., Draxl, C., Mirocha, J. D., Muradyan, P., Ghate, V. P., Optis, M., and Lemke, A.: Workshop on Research Needs for Offshore Wind Resource Characterization: Summary Report, Tech. rep., Pacific Northwest National Lab.(PNNL), Richland, WA (United States), 2019.

Shepherd, T. J., Barthelmie, R. J., and Pryor, S. C.: Sensitivity of Wind Turbine Array Downstream Effects to the Parameterization Used in WRF, Journal of Applied Meteorology and Climatology, 59, 333–361, https://doi.org/10.1175/JAMC-D-19-0135.1, 2020.

Siedersleben, S. K., Platis, A., Lundquist, J. K., Djath, B., Lampert, A., Bärfuss, K., Cañadillas, B., Schulz-Stellenfleth, J., Bange, J., Neumann, T., and Emeis, S.: Turbulent Kinetic Energy over Large Offshore Wind Farms Observed and Simulated by the Mesoscale Model WRF (3.8.1), Geoscientific Model Development, 13, 249–268, https://doi.org/10.5194/gmd-13-249-2020, 2020.

Skamarock, W. C., Klemp, J. B., Dudhia, J., Gill, D. O., and Liu, Z.: A Description of the Advanced Research WRF Model Version 4.3, 2021.

Storm, B. and Basu, S.: The WRF Model Forecast-Derived Low-Level Wind Shear Climatology over the United States Great Plains, Energies, 3, 258–276, https://doi.org/10.3390/en3020258, 2010.

Stull, R. B.: An Introduction to Boundary Layer Meteorology, vol. 13, Springer Science & Business Media, 1988.

Tewari, M., Chen, F., Wang, W., Dudhia, J., LeMone, M., Mitchell, K., Ek, M., Gayno, G., Wegiel, J., et al.: Implementation and Verification of the Unified NOAH Land Surface Model in the WRF Model (Formerly Paper Number 17.5), in: Proceedings of the 20th Conference on Weather Analysis and Forecasting/16th Conference on Numerical Weather Prediction, Seattle, WA, USA, vol. 14, 2004.

Thompson, G., Field, P. R., Rasmussen, R. M., and Hall, W. D.: Explicit Forecasts of Winter Precipitation Using an Improved Bulk Microphysics Scheme. Part II: Implementation of a New Snow Parameterization, Monthly Weather Review, 136, 5095–5115, https://doi.org/10.1175/2008MWR2387.1, 2008.

Tomaszewski, J. M. and Lundquist, J. K.: Simulated Wind Farm Wake Sensitivity to Configuration Choices in the Weather Research and Forecasting Model Version 3.8.1, Geoscientific Model Development, 13, 2645–2662, https://doi.org/10.5194/gmd-13-2645-2020, 2020.

Vanderwende, B. J., Kosović, B., Lundquist, J. K., and Mirocha, J. D.: Simulating Effects of a Wind-Turbine Array Using LES and RANS, Journal of Advances in Modeling Earth Systems, 8, 1376–1390, https://doi.org/10.1002/2016MS000652, 2016.

Vineyard Wind: Vineyard Wind Receives Record of Decision for First in the Nation Commercial Scale Offshore Wind Project, https://www.vineyardwind.com/press-releases/2021/5/11/vineyard-wind-receives-record-of-decision, 2021.

Volker, P. J. H., Badger, J., Hahmann, A. N., and Ott, S.: The Explicit Wake Parametrisation V1.0: A Wind Farm Parametrisation in the Mesoscale Model WRF, Geoscientific Model Development, 8, 3715–3731, https://doi.org/10.5194/gmd-8-3715-2015, 2015.

White House: FACT SHEET: Biden Administration Jumpstarts Offshore Wind Energy Projects to Create Jobs, https://www.whitehouse.gov/briefing-room/statements-releases/2021/03/29/fact-sheet-biden-administration-jumpstarts-offshore-wind-energy-projects-to-create-jobs/, 2021.

Yang, B., Qian, Y., Berg, L. K., Ma, P.-L., Wharton, S., Bulaevskaya, V., Yan, H., Hou, Z., and Shaw, W. J.: Sensitivity of Turbine-Height Wind Speeds to Parameters in Planetary Boundary-Layer and Surface-Layer Schemes in the Weather Research and Forecasting Model, Boundary-Layer Meteorology, 162, 117–142, https://doi.org/10.1007/s10546-016-0185-2, 2017.

Yang, B., Berg, L. K., Qian, Y., Wang, C., Hou, Z., Liu, Y., Shin, H. H., Hong, S., and Pekour, M.: Parametric and Structural Sensitivities of Turbine-Height Wind Speeds in the Boundary Layer Parameterizations in the Weather Research and Forecasting Model, Journal of Geophysical Research: Atmospheres, 124, 5951–5969, https://doi.org/10.1029/2018JD029691, 2019.

Yang, Q., Berg, L. K., Pekour, M., Fast, J. D., Newsom, R. K., Stoelinga, M., and Finley, C.: Evaluation of WRF-Predicted Near-Hub-Height Winds and Ramp Events over a Pacific Northwest Site with Complex Terrain, Journal of Applied Meteorology and Climatology, 52, 1753–1763, https://doi.org/10.1175/JAMC-D-12-0267.1, 2013.

Zhang, X., Bao, J.-W., Chen, B., and Grell, E. D.: A Three-Dimensional Scale-Adaptive Turbulent Kinetic Energy Scheme in the WRF-ARW Model, Monthly Weather Review, 146, 2023–2045, https://doi.org/10.1175/MWR-D-17-0356.1, 2018.